Tectonophysics 765 (2019) 226–248

Contents lists available at ScienceDirect

Tectonophysics

journal homepage: www.elsevier.com/locate/tecto

Tectonic and sediment provenance evolution of the South Eastern Pyrenean foreland basins during rift margin inversion and orogenic uplift

M.L. Odlum[a,*], D.F. Stockli[a], T.N. Capaldi[a], K.D. Thomson[a], J. Clark[b], C. Puigdefàbregas[c], A. Fildani[b]

[a] Department of Geological Sciences, Jackson School of Geosciences, University of Texas at Austin, Austin, TX 78712, USA
[b] Equinor, Research Center Austin, 6300 Bridge Point Parkway, Austin, TX, USA
[c] Departament de Geodinámica i Geofísica, Universitat de Barcelona, Barcelona, Spain

ARTICLE INFO

Keywords:
Foreland basins
Fold-and-thrust belts
Sedimentary provenance
Detrital zircon U-Pb geochronology
Detrital rutile U-Pb geochronology
Detrital thermochronology

ABSTRACT

The Cretaceous to Oligocene detrital record in the southern Eastern Pyrenees is utilized to address the degree to which precursor basin architecture and hyper-extensional rift structures impacted subsequent sedimentary provenance and dispersal systems and foreland basin evolution. This study presents new isotopic provenance analysis of detrital zircon U—Pb and (U—Th)/He double-dating, and detrital rutile U—Pb and trace element geochemistry to track sediment provenance evolution. Late Cretaceous-Paleocene sediments show zircon with dominantly Variscan U—Pb and Jurassic-Early Cretaceous ZHe cooling ages that are derived from southeastern Catalan Coastal Ranges and eastern Corsica-Sardinia regions, and localized structural inversion along inherited Mesozoic extensional faults and erosional recycling of syn-rift sediments. Eocene deposits have multimodal U—Pb ages that stratigraphically upsection change to unimodal Variscan ages, with the appearance and upsection increase in Pyrenean ZHe ages, and increase in Variscan aged detrital rutile that record a significant shift in sediment source area to northern sources recording exhumation and unroofing of the Axial Zone Paleozoic basement sources, and development of new ramp-flat style structures in the Southern Pyrenean Zone fold-thrust belt. During the Oligocene, incipient foreland basin deposits were cannibalized and recycled into the foreland basin as thrusting advanced toward the foreland. The Eastern Pyrenean foreland basin records a different provenance history from Central Pyrenean Tremp Basin, suggesting the basins were segmented throughout the Late Cretaceous to Oligocene, while the Ripoll and Ager basins appear to have shared similar source areas. The sediment provenance evolution coupled with Pyrenean fault activity and shortening rates, hinterland exhumation, foreland basin subsidence, and climate proxies presents a detailed dataset to understand these relationships within the Eastern Pyrenean orogenic system and highlight the dominant control precursor basins and structural inheritance has on the subsequent fold-thrust belts and foreland basin evolution.

1. Introduction

Fault reactivation and basin inversion can significantly impact foreland basin architecture, sediment provenance, and sediment dispersal patterns in inverted rift systems (e.g. Fildani and Hessler, 2005; Horton et al., 2010; Romans et al., 2010; Fosdick et al., 2014; Perez et al., 2016; Vacherat et al., 2017). There remains limited understanding of sediment provenance and dispersal evolution with relation to deformation and exhumation patterns through time in foreland basins that are strongly influenced by preexisting structures. A significant obstacle in understanding many of these systems is preservation of precursor crustal architecture as contractile tectonics often destroys and/or significantly overprints it. Fundamental questions remain regarding the tectonic inversion of highly-attenuated and segmented rift margins and the impact on source-to-sink systems, including: 1) what governs variations in provenance and sediment routing of these systems through time? 2) When does orogenic topography overpower the inherited rift architecture and become the dominant source to the peripheral foreland basins? 3) What is the style of deformation and exhumation patterns in the fold-and-thrust belt through time, and how do present day structurally segmented basins initiate and evolve through time?

The Pyrenees orogenic system is an exemplar setting to address the feedbacks and thresholds during the transition from extensional rift

* Corresponding author.
E-mail address: modlum@utexas.edu (M.L. Odlum).

https://doi.org/10.1016/j.tecto.2019.05.008
Received 1 February 2019; Received in revised form 27 April 2019; Accepted 9 May 2019
Available online 21 May 2019
0040-1951/ © 2019 Elsevier B.V. All rights reserved.

structures and associated basin systems to the superimposed collision-driven shortening and foreland basin development. The crustal and lithospheric structure of the Pyrenees is well-constrained by extensive geological studies (e.g. Puigdefàbregas and Souquet, 1986; Muñoz, 1992; Teixell, 1998; Vergés et al., 1995, 2002; Mouthereau et al., 2014; Teixell et al., 2016; Grool et al., 2018; Ternois et al., 2019), ECORS deep seismic profiles (e.g. Choukroune, 1989; Roure et al., 1989; Daignières et al., 1994), and seismic tomography (e.g. Souriau et al., 2008; Chevrot et al., 2014; Wang et al., 2016). The Pyrenees preserve a record of their entire post-Variscan tectonic evolution, including Jurassic to Cretaceous rift structures and basins, variations in hinterland structural styles across and along strike with well-established deformation histories, basement-involved and salt-detached portions of the fold-and-thrust-belt, and a complete Cretaceous through Oligocene foreland basin succession. An extensive dataset of sedimentologic, stratigraphic, petrographic, structural, and geo- and thermochronometric constraints for the Pyrenean region provides a unique opportunity to explore the impacts of inherited rift-related structures and basins on the subsequent evolution of an inverted continental margin and superimposed collisional orogenic system and foreland basin.

The foreland basin(s) in the southeastern Pyrenees are structurally isolated and difficult to compare with the more extensively studied provenance and source-to-sink systems of the Tremp, Ager, and Jaca basins in the central and western Spanish Pyrenees (e.g. Whitchurch et al., 2011; Roigé et al., 2016, 2017; Clark et al., 2017; Thomson et al., 2017). The Eastern Pyrenees were strongly affected by Late Cretaceous inversion tectonics and by diachronous Cenozoic collisional shortening. The Ripoll and Ebro foreland basins in the southeastern Pyrenees straddle the intersection of the Pyrenean orogen and Catalan Coastal Range, linking the Pyrenees to the Alpine regions to the east (e.g. Alps, Corsica, Sardinia) and the foreland basin deposits record the landscape before the opening of the Gulf of Lion and Valencia Trough during western Mediterranean slab roll back in the Miocene (e.g. Gueguen et al., 1998; Roca et al., 1999; Séranne, 1999; Rosenbaum et al., 2002; Gunnell et al., 2008).

This study investigates the Cretaceous to Oligocene foreland basin sedimentary record of the southeastern Pyrenean basins to reconstruct source-to-sink systems in the fold-and-thrust belt and foreland basin. We present a suite of isotopic provenance tracers to constrain the relationships between hinterland exhumation and erosion, sediment routing, and fold-and-thrust belt and foreland basin system evolution. Understanding the mechanisms of inversion and role of inherited structures impart on orogenic systems has broader impact on hydrocarbon systems, regional deformation and structural reactivation, seismicity, and tectonics models globally. In addition, this work provides valuable analogs for understanding the geological evolution of similar tectonic settings, such as the Atlas Mountains, Caucasus, Taiwan, and many segments of the Andes (e.g. Lacombe and Mouthereau, 2002; Babault et al., 2013; Cowgill et al., 2016; Perez et al., 2016).

2. Geologic setting

2.1. Tectonic provinces

The Pyrenees Mountains are an east-west trending orogenic belt along the border of France and Spain and are the westernmost expression of the Alpine-Himalayan orogenic belt (Fig. 1). The Pyrenean orogeny resulted from the oblique convergence and collision between the Iberian microplate with the Eurasian plate (Puigdefàbregas and Souquet, 1986; Choukroune, 1989; Muñoz, 1992; Vergés et al., 2002; Vissers and Meijer, 2012; Grool et al., 2018; Teixell et al., 2018). The Pyrenees, a doubly-vergent orogenic wedge, can be divided into five distinct structural zones (Fig. 1): 1) the undeformed retro-wedge foreland basin, Aquitaine basin, north of Pyrenees; 2) the North Pyrenean Zone (NPZ), a narrow (25–35 km wide) retro-wedge fold-and-thrust belt, characterized by steep north-vergent reverse faults which exhumed Paleozoic basement and highly deformed and partially metamorphosed Mesozoic strata (e.g. Ford et al., 2016); 3) the Axial Zone is the structurally thickened core of the Pyrenees characterized by south-vergent antiformal stack of thrust sheets composed of Neoproterozoic to Paleozoic crystalline basement (e.g. Muñoz, 1992); 4) the South Pyrenean Zone, a south-verging thin-skinned ramp-flat fold-and-thrust belt that translated Mesozoic and Cenozoic basin fill above a Triassic evaporitic décollement (e.g. Puigdefàbregas et al., 1992; Vergés et al., 2002); 5) the pro-wedge foreland basin, Ebro Basin, extending from the south Pyrenean fold-and-thrust belt to the Catalan Coastal Ranges and Iberian Range (Fig. 1). Total shortening in the Eastern Pyrenees is estimated at a minimum of ~111 km, excluding closure of the exhumed mantle domain (Vergés, 1993; Grool et al., 2018).

The Catalan Coastal Ranges (CCR) (Fig. 1) are a predominantly basement-involved fold-and-thrust belt system that formed during the Late Cretaceous-early Oligocene and was subsequently compartmentalized into two main horsts and several grabens during the Late Oligocene to Miocene opening of the Valencia Trough (Roca et al., 1999; Juez-Larré and Andriessen, 2006). The CCR exposes four major tectonostratigraphic units, 1) the Paleozoic basement including Variscan felsic plutonic rocks; 2) autochthonous to para- autochthonous Mesozoic sedimentary cover; 3) allochthonous thrust sheets carrying the inverted Mesozoic rift basin; and 4) syn-tectonic Cenozoic foreland basin deposits (e.g. Juez-Larré and Andriessen, 2006 and references within) (Fig. 1).

2.2. Deformation phases

The tectonic evolution of the Pyrenees can be subdivided into five significant deformational phases since the Late Paleozoic. These are 1) the Variscan orogeny (e.g., Respaut and Lancelot, 1983; Vissers, 1992; Gleizes et al., 1997; Olivier et al., 2004, 2008; Denèle et al., 2014), 2) widespread, diffuse post-Variscan Permian and Triassic rifting (e.g., Stampfli and Borel, 2002), 3) Early Cretaceous rifting and hyperextension between the Iberian and European plates (e.g., Debroas, 1987, 1990; Lagabrielle and Bodinier, 2008; Jammes et al., 2009; Lagabrielle et al., 2010; Clerc et al., 2012; Tugend et al., 2015; Ford et al., 2016), 4) Late Cretaceous rift inversion and Cenozoic Pyrenean collisional orogeny (e.g., Choukroune, 1989; Muñoz, 1992; Mouthereau et al., 2014 and references within; Ternois et al., 2019) and 5) Miocene extension and opening of the Valencia Trough and Gulf of Lion that destroyed the eastern termination of the Pyrenean orogen (e.g. Gueguen et al., 1998; Roca et al., 1999; Séranne, 1999; Rosenbaum et al., 2002; Gunnell et al., 2008, 2009). Several studies have shown that pre-Cenozoic inherited structural grain, discrete structures, and basin configuration and basin fill governed or significantly influenced the structural evolution of collision orogenesis in the Pyrenees (e.g., Mouthereau et al., 2014; Vacherat et al., 2016; Ternois et al., 2019).

The Late Cretaceous-Oligocene fold-and-thrust belt evolution had three distinct periods of shortening related to the progressive emplacement of different thrust sheets in the southeastern portion of the Pyrenees: 1) ~83 to 55 Ma: inversion of pre-existing Early Cretaceous rift basins and emplacement of the structurally highest Upper Pedraforca thrust sheets, with overall low shortening rates of < 0.5 mm/yr (Vergés et al., 1995); 2) 54–44 Ma: thrusting and imbrication on the Lower Pedraforca thrust sheet with highest rates of shortening, 4–4.4 mm/yr (Vergés et al., 1995); and 3) ~44 Ma to ~30 Ma: deformation along the frontal thrusts accommodated along the Vallfogona Thrust which became emergent ~43.5 Ma, and imbricate thrusting in the hinterland Axial Zone at shortening rates of 1.5–2.6 mm/yr (Burbank et al., 1992; Vergés et al., 1995, 2002; Ramos et al., 2002; Metcalf et al., 2009; Vacherat et al., 2017 and references within).

2.3. Stratigraphy of the south Eastern Pyrenees

Extensive study of the stratigraphy of the Eastern Pyrenees foreland

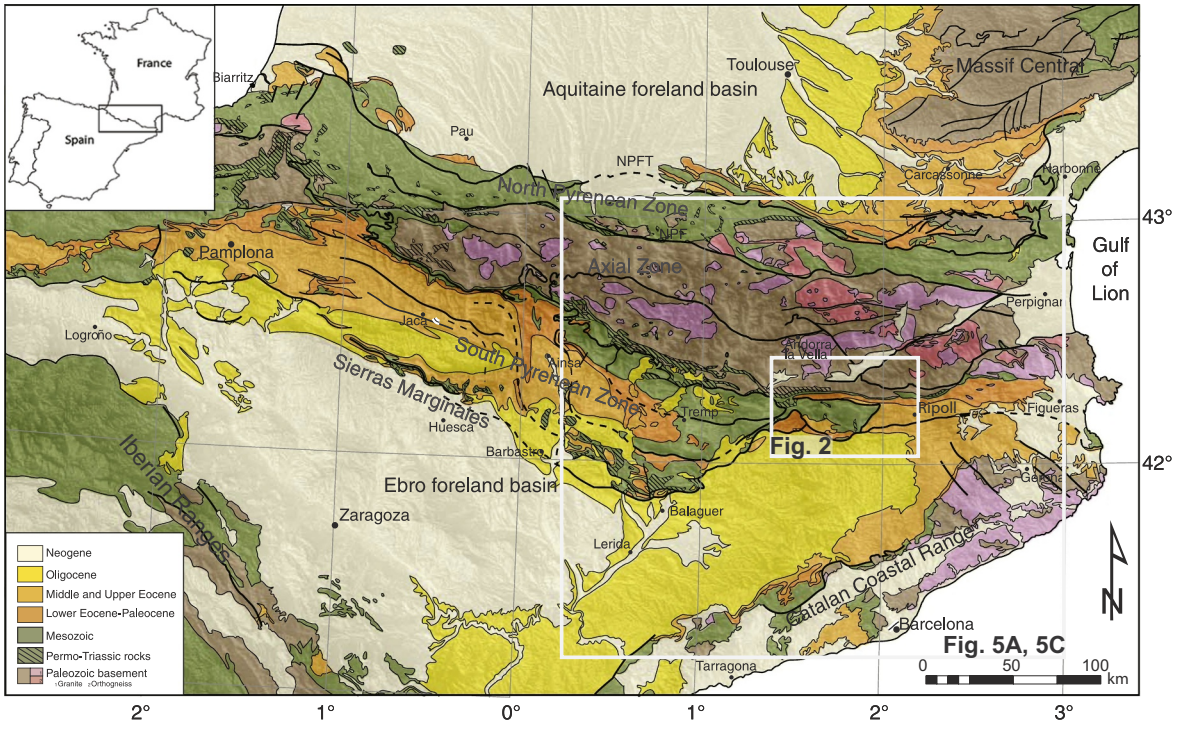

Fig. 1. Map showing tectonic and geologic framework of the Pyrenees (1:106 scale) modified from Mouthereau et al., 2014. Inset boxes show locations of Figs. 2 and 5A and C.

basin (Muñoz, 1985; Puigdefàbregas et al., 1986; Martinez et al., 1989; Burbank et al., 1992) has established a well-defined chronostratigraphic framework using magnetostratigraphy and biostratigraphy summarized by Vergés et al., 2002 (e.g., Burbank et al., 1992; Serra-Kiel et al., 1994; Vergés and Burbank, 1996; Serra-Kiel et al., 1998). The following section presents a summary of the key stratigraphic intervals that record the history of Pyrenean orogenesis from Late Cretaceous inversion through the Paleogene collisional orogenesis that were sampled and analyzed in this study.

2.3.1. Adraén section: Upper Cretaceous strata

The Santonian-Campanian Spell Adraèn Formation consists of white quartz conglomerate, sandstone, and occasional thin shale interbeds (Fig. 2; Mey et al., 1968). The overlying Bona Formation consists of bioclastic limestone, which is highly fossiliferous, containing mainly rudists. The base of the Bona Formation contains local sandy siliciclastic intervals (Mey et al., 1968).

2.3.2. Ripoll Basin

The Ripoll Basin is the easternmost basin within the South Pyrenean Zone (Fig. 2) and contains stratigraphy consisting of Upper Cretaceous to Upper Eocene syn-tectonic foreland basin deposits (Puigdefàbregas et al., 1986; Puigdefàbregas and Souquet, 1986; Muñoz et al., 1986; Ramos et al., 2002; Serra-Kiel et al., 2003). We sampled the Bagà and Sant Jaume composite sections defined by Burbank et al. (1992) in the Ripoll Syncline for detrital mineral analysis (Figs. 2, 3).

2.3.2.1. Bagà section: Upper Cretaceous-Ypresian strata. The Bagà section is in the hanging wall of the Vallfogona thrust between the Axial Zone to the north and the outcrop of the Pedraforca thrust sheet to the south (Fig. 2). The section contains Permo-Triassic rhyolites and fluvial red sandstone and siltstone beds unconformably deposited on Axial Zone basement (Devonian schists), Cretaceous carbonate and sandstone, Paleocene fluvial sandstone and paleosol beds, and Eocene Cadi and Corones sequences (Fig. 3).

The Cretaceous strata in the Bagà section are ~100 m thick with an upsection transition from marine to lagoon facies with paleocurrents directions toward the west (Fig. 3; Oms et al., 2016). During the Early Maastrichtian tidal currents were confined to an E-W-oriented, elongate foreland basin trough (Riera et al., 2010). The Late Cretaceous-Paleocene Tremp Formation in the Bagà section consist of red siltstone, overlain by poorly sorted silty to very fine sandstone with granule-pebble floating clast paleosols, overlain by red fluvial fine to medium grained sandstone and siltstone (Fig. 3).

The earliest Eocene deposits are the transgressive Cadi sequence, composed of the shallow lacustrine marls and Cadi Limestone at the base that grade stratigraphically upsection into the deeper water facies of the Sagnari Marl (Fig. 3; Puigdefàbregas et al., 1986; Burbank et al., 1992). The Sagnari Marl is interpreted to mark an intial deepening of the basin associated with early flexural subsidence during initial thrust loading from the north (Burbank et al., 1992; Vergés et al., 1998). The Cadi sequence is overlain by the regressive Corones sequence. The Corones Formation is a ~700 m thick southward prograding deltaic sequence that grades upward from shallow marine to fluvial deposits with N to S directed paleocurrents (Fig. 3) (Puigdefàbregas et al., 1986; Burbank et al., 1992). The top of the Corones Formation is characterized by algal limestones (Puigdefàbregas et al., 1986; Burbank et al., 1992). The Armàncies sequence is stratigraphically above the Corones sequence and is composed of slope shale deposits with carbonate turbidites and slope breccias that contain carbonate clasts from the Cadi sequence in the lower part of the formation, commonly referred to as megaturbidites (Puigdefàbregas et al., 1986; Burbank et al., 1992).

2.3.2.2. Sant Jaume section: Lutetian-Priabonian strata. The Sant Jaume section is in the southern limb of the Ripoll syncline (Fig. 2). The ~3100 m thick section spans much of the syntectonic sequence in the Eastern Pyrenees (Fig. 3). In the south, the section is delimited at its base by the Vallfogona thrust which carries the Campdevanol Formation in the hanging wall (Fig. 4). There is a shallowing trend upsection with deep marine turbidites, open marine prodelta and delta front facies evolving into delta plain facies with low-sinuosity braided, rivers interbedded with alluvial fan facies (Ramos et al., 2002).

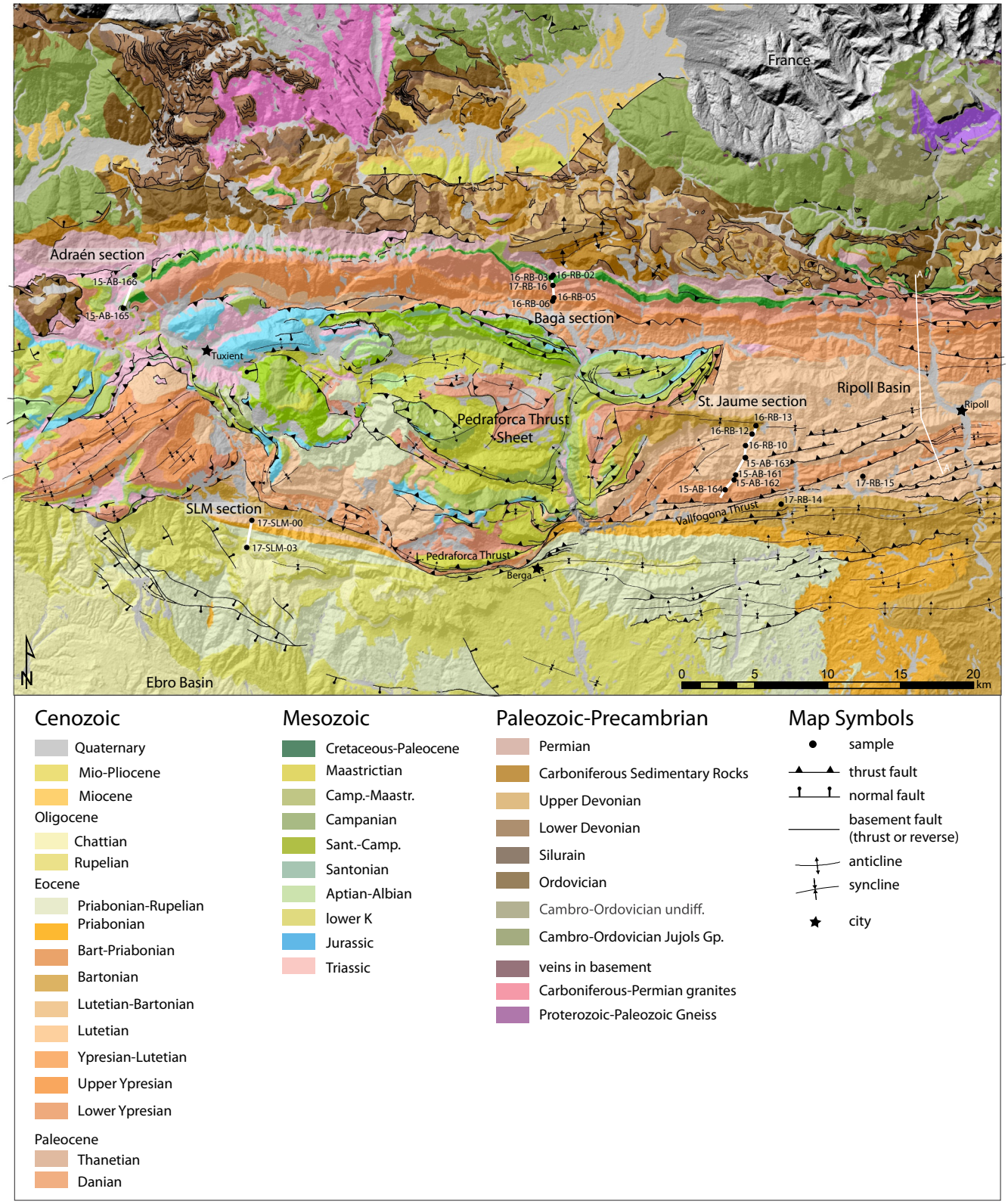

Fig. 2. Geologic map of the Eastern Pyrenees with sample locations (black circles), stratigraphic section (white lines; in this figure) and cross-section in Fig. 4 (A-A′ line; Fig. 3). Modified from the Institut Cartogràfic i Geològic de Catalunya (ICGC) 1:50,000 scale shapefiles.
ASTER GDEM data courtesy of NASA and METI.

Unconformities within the section were interpreted to mark thrust-related deformation including the imbrication of the Upper and Lower Pedraforca thrust sheets (~83–47 Ma), out-of-sequence thrusting in the Axial Zone (~50–25 Ma), and the thrusting along the Vallfogona thrust (~44–30 Ma) that caused folding of the Ripoll syncline (Puigdefàbregas et al., 1986; Burbank et al., 1992; Ramos et al., 2002).

The Campdevanol sequence is up to 900 m thick and composed of siliciclastic turbidites with a west directed paleoflow (Puigdefàbregas

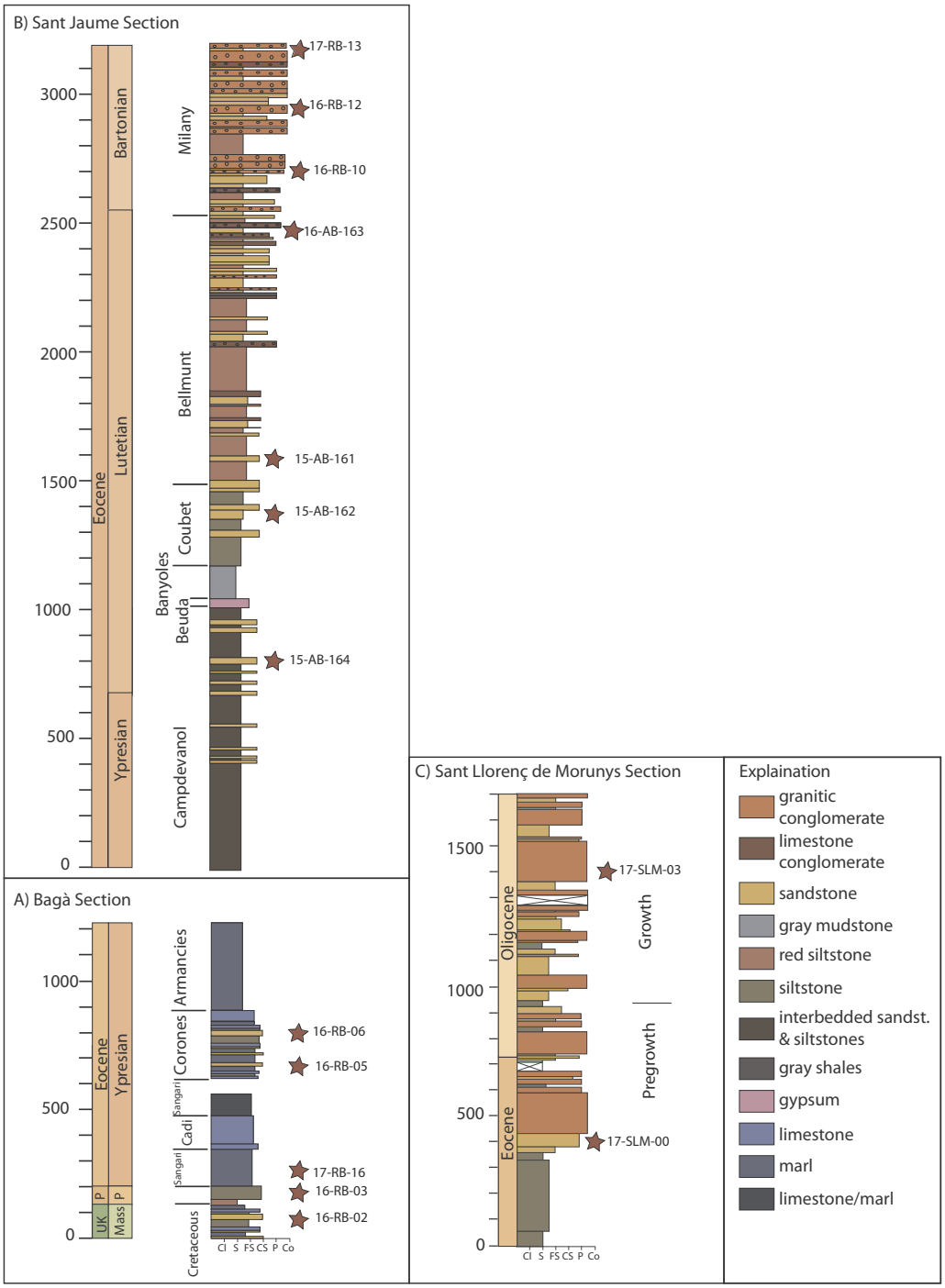

Fig. 3. Schematic stratigraphic sections of the Ripoll Basin and Sant Llorenç de Morunys sections with sample locations (red stars). (A) Bagà Upper Cretaceous-Paleocene-Lower Eocene mixed marine non-marine section. (B) Sant Jaume Eocene marine to non-marine sections (modified from Burbank et al., 1992). (C) The Sant Llorenç de Morunys Eocene to Oligocene non-marine section (modified from Carrigan et al., 2016). (For interpretation of the references to color in this figure legend, the reader is referred to the web version of this article.)

et al., 1986). Both coarse and fine-grained turbidite beds are interbedded with siltstone, and some thin layers (< 5 m thick) of secondary gypsum (Carrillo et al., 2014). The low faunal content suggests a restricted, hypersaline basin during deposition (Puigdefàbregas et al., 1986; Carrillo et al., 2014). The Beuda sequence is composed of up to 70 m thick alabastrine gypsum evaporites (Fig. 3; Puigdefàbregas et al., 1986; Carrillo et al., 2014) suggesting constriction of the basin (Vergés et al., 1992; Carrillo et al., 2014).

The Bellmunt sequence is characterized by medium grained sandstones and pebble conglomerates interpreted as south-ward prograding fluvial and deltaic deposits (Fig. 3; Puigdefàbregas et al., 1986) with a dominant west directed paleoflow direction that gradually changes to a southwest directed paleoflow direction upsection (Ramos et al., 2002). The Bellmunt sequence is composed of the: Banyoles Formation, prodelta blue marls with micritic and turbidite beds (Carrillo et al., 2014); the Coubet Fomation, shallow marine deltaic deposits of grey sandstones with some thin (< 5 m) beds of micrite and secondary gypsum; and the Bellmunt Formation, red and brown medium-coarse grained sandstones and bioturbated red mudstones, with pebble-gravel conglomerates (Fig. 3; Carrillo et al., 2014). The Milany sequence is

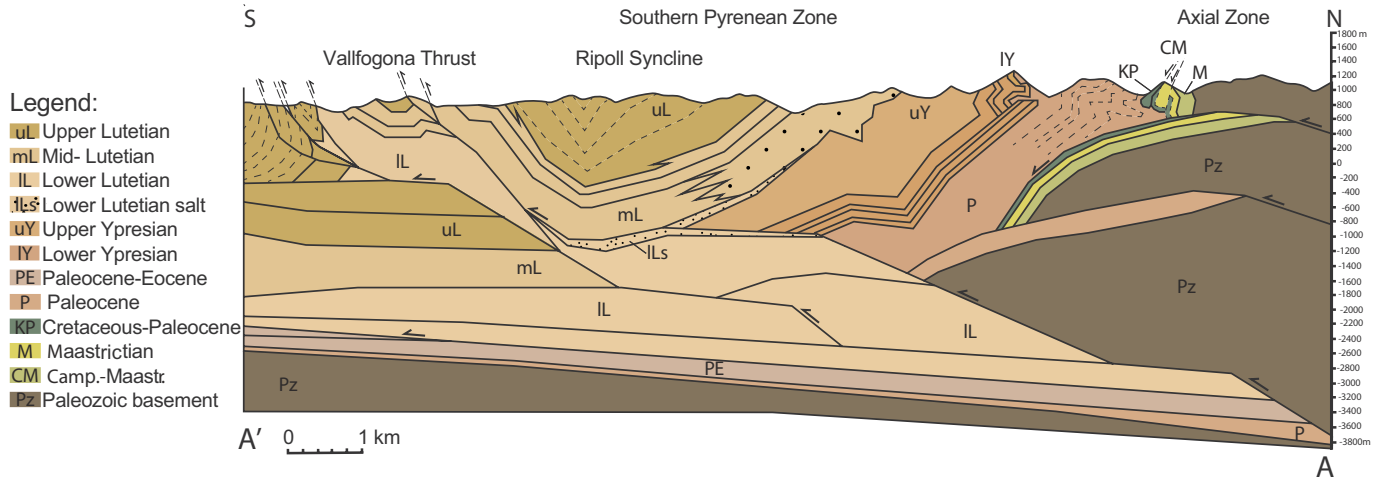

Fig. 4. Cross-section across the Ripoll Basin, displaying Axial zone basement thrust and Vallfogona ramp-flat thrust within Eocene stratigraphy (ICGC 1:25,000 Ripoll map Sheet 256-1-2).

characterized by alluvial fan deposits and the first appearance of granitic clasts at its base (Burbank et al., 1992). These clasts have been interpreted as being derived from the uplifting and denuding Axial Zone crystalline basement during large-scale out-of-sequence thrusting (Puigdefàbregas et al., 1986; Burbank et al., 1992; Ramos et al., 2002). Paleoflow directions in the Milany sequence change upsection from southwest- to southward-directed paleo-flow (Ramos et al., 2002).

2.3.3. Sant Llorenç de Morunys: Upper Priabonian-Oligocene strata

The Sant Llorenç de Morunys section consists of ~2.5 km of Upper Eocene-Oligocene alluvial conglomerates of the Berga Formation (Fig. 3; Riba, 1976; Mató et al., 1994; Ford et al., 1997; Carrigan et al., 2016). The Berga conglomerate lies in the footwall of the Vallfogona Thrust and forms a package of growth strata with beds thickening and fanning toward the south (Riba, 1976; Ford et al., 1997). The folding responsible for the growth strata geometry is directly related to motion on the Vallfogona Thrust (Ford et al., 1997; Suppe et al., 1997).

While the South Pyrenean Zone stratigraphy and deformation history are well defined (e.g., Burbank et al., 1992; Puigdefàbregas et al., 1992; Vergés et al., 1992, 2002; López-Blanco et al., 2000; Gómez-Paccard et al., 2012), the sedimentary provenance and thermal record of the hinterland are poorly constrained. This study uses multiple provenance techniques to constrain the sediment provenance evolution and the basin-scale depositional history in the context of the well-constrained hinterland tectonic history. This study provides an important dataset linking deformation, sedimentation, sediment provenance evolution, and exhumation history of the hinterland and helps to further elucidate the feedbacks that exist between tectonic deformation and foreland basin deposition.

3. Methodology

Samples were collected from Upper Cretaceous to Oligocene strata along four sections in the Eastern Pyrenees (Figs. 2, 3). Samples 15-AB-165 and 15-AB-166 are Upper Cretaceous sandstones near the village of Adraén. Samples 16-RB-02, 16-RB-03, 17-RB-16, 16-RB-05, and 16-RB-06 were taken in the Bagà section of Burbank et al. (1992). Samples 15-AB-161, -162, -163, -164, 16-RB-10, and 16-RB-12 were taken in the Sant Jaume section of Burbank et al. (1992) along the road to Sant Jaume de Frontyanà. Samples 16-RB-14 and 16-RB-15 were taken south of the Vallfogona Thrust along the road between Borredà and Les Llosses. Samples 17-SLM-00 and 17-SLM-03 were taken from conglomerates in Sant Llorenç de Morunys. Sandstone samples (2–5 kg) were collected targeting sandstones with a consistent medium grained sand to minimize effects of hydrodynamic grain size fractionation (e.g. Malusà et al., 2016). Samples were separated following standard crushing, grinding, and heavy mineral separation techniques. All U–Pb analysis and (U–Th)/He analysis were conducted at the UTChron facility at the University of Texas at Austin.

3.1. Detrital zircon U–Pb and (U–Th)/He methodology

Detrital zircon (DZ) analysis was conducted by depth-profile laser ablation–inductively coupled plasma–mass spectrometry (LA-ICP-MS) U–Pb dating following procedures described in Hart et al. (2016). DZ U–Pb ages record crystallization and high-temperature metamorphism (~800–1110 °C) of the igneous or metamorphic protolith (e.g. Gehrels, 2012; Schoene, 2014). Several studies that have used DZ U–Pb, ZHe, and/or ZFT to assess the sedimentary provenance of the central and western southern Pyrenees foreland basin deposits and have characterized the source area zircon signatures (Fig. 5A, B; Whitchurch et al., 2011; Beamud et al., 2011; Filleaudeau et al., 2011; Bosch et al., 2016; Thomson et al., 2017; Vacherat et al., 2017). DZ U–Pb ages were binned into groups based on the main components present in the age spectra that reflect important geodynamic phases in the Pyrenees and western European region. The age spectra were divided as follows: Cretaceous (66–145 Ma), Post-Variscan (145–280 Ma), Variscan (280–420 Ma), Cambrian-Silurian (420–520 Ma), Cadomian-Pan African (520–700 Ma), Neoproterozoic (700–900), Kibaran (900–1200 Ma), and Mesoproterozoic-Archean (> 1200 Ma). DZ U–Pb results are summarized in terms of percentages of components in Table 1, Kernel Density Estimators (KDEs), and histograms in Fig. 6 and tabulated in dataset S3 in the Supplementary material.

Zircon (U–Th)/He (ZHe) analyses were conducted following procedures described in Wolfe and Stockli (2010)and Hart et al., (2017). ZHe ages record cooling below ~180 °C (Reiners, 2005; Wolfe and Stockli, 2010), providing information about the thermal and exhumation history of the source terrane. In fold-and-thrust belts, ZHe is a robust method to constrain the timing of major thrust motion, recording the cooling along thrust ramps, and is also less susceptible than apatite (U-Th)/He to resetting due to burial and erosion (Reiners et al., 2005). It is a particularly useful technique for distinguishing source regions in tectonic settings that have non-unique source DZ U–Pb signatures but different thermal histories and/or significant sediment recycling (e.g., Reiners et al., 2005; Campbell et al., 2005; Saylor et al., 2012). ZHe ages were binned into groups reflecting important tectono-thermal phases in Pyrenean region (e.g., Thomson et al., 2017; Vacherat et al., 2017). The bins were divided as follows: Pyrenean orogeny (< 70 Ma),

Table 1
Detrital zircon U—Pb results summarized in component percentages.

Sample	Formation	n	Cretaceous	Post-Variscan	Variscan	Cambrian-Silurian	Cadomian	Neoproterozoic	Kibaran	Mesoproterozoic-Archean
			66–145 Ma	145–280 Ma	280–420 Ma	420–520 Ma	520–700 Ma	700–900 Ma	900–1200 Ma	> 1200 Ma
15-AB-166	Adraen	122	2.5%	6.6%	37.7%	6.6%	18.9%	9.8%	4.9%	13.1%
15-AB-165	Bona	132	4.5%	1.5%	59.8%	7.6%	11.4%	3.8%	3.8%	7.6%
16-RB-02	Late Cret.	129	0.0%	0.8%	27.9%	10.9%	28.7%	14.7%	7.0%	10.1%
16-RB-03	Garumnian	97	0.0%	1.0%	52.6%	16.5%	17.5%	2.1%	2.1%	8.2%
16-RB-16	Sangari	141	0.7%	2.8%	13.5%	14.2%	24.8%	2.8%	12.1%	29.1%
16-RB-05	L. Corones	125	0.0%	2.4%	7.2%	12.8%	28.0%	18.4%	18.4%	12.8%
16-RB-06	U. Corones	127	0.0%	3.1%	18.1%	14.2%	31.5%	7.9%	10.2%	15.0%
15-AB-164	Campdevanol	129	0.0%	1.6%	28.7%	24.8%	22.5%	7.8%	3.9%	10.9%
15-AB-162	Coubet	120	0.0%	0.0%	20.8%	24.2%	22.5%	10.0%	6.7%	15.8%
15-AB-161	L. Bellmunt	121	0.0%	1.7%	10.7%	32.2%	23.1%	4.1%	11.6%	16.5%
15-AB-163	U. Bellmunt	133	0.0%	1.5%	15.0%	15.0%	26.3%	3.8%	13.5%	24.8%
16-RB-10	L. Milany	125	0.0%	0.8%	25.6%	8.0%	29.6%	9.6%	14.4%	12.0%
16-RB-12	Milany	113	0.0%	4.4%	95.6%	0.0%	0.0%	0.0%	0.0%	0.0%
16-RB-13	U. Milany	147	0.0%	2.0%	93.2%	1.4%	1.4%	0.0%	0.0%	2.0%
16-RB-14	Bellmunt	144	0.0%	2.8%	56.3%	9.7%	13.9%	3.5%	4.9%	9.0%
16-RB-15	Bellmunt	138	0.0%	2.2%	91.3%	0.7%	2.9%	0.7%	0.7%	1.4%
17-SLM-00	Berga	141	0.0%	1.4%	54.6%	9.2%	19.9%	0.7%	5.0%	9.2%
17-SLM-03	Berga	134	0.0%	1.5%	35.8%	10.4%	20.9%	9.0%	9.0%	13.4%

Late Cretaceous inversion (85–100 Ma), Early Cretaceous rifting (100–85 Ma), Jurassic (145–200 Ma), and Triassic-Paleozoic (> 200 Ma). ZHe results are summarized in terms of percentage of components in Table 2, KDEs and histograms in Fig. 7, lag times in Fig. 8, and tabulated in dataset S3. Double-dating age relationships are summarized in Fig. 7. Grains with ZHe ages younger than the depositional age of the sample are excluded because these grains may be partially reset by burial, or owing to variable diffusion kinetics based on radiation damage, radiogenic parent nuclide zoning, or grain size (e.g. Reiners, 2005; Hourigan et al., 2005; Guenthner et al., 2013 (see Supplementary material, S3).

3.2. Detrital rutile U—Pb and trace element methodology

Rutile U—Pb is a medium-temperature thermochronometer (Tc~450–600 °C) whose U—Pb ages record the age of the most recent greenschist facies or higher-grade metamorphism, or exhumation and cooling from middle and lower crustal levels (e.g. Kooijman et al., 2010; Smye et al., 2018). Rutile geochemistry and Zr-in-rutile thermometry yield diagnostic data on the lithology and metamorphic facies of sediment source areas, even in highly modified sandstones that may have lost significant amounts of provenance information (e.g. Zack et al., 2004; Zack et al., 2011; Meinhold, 2010; Triebold et al., 2012). Detrital rutile (DR) grains were analyzed by LA-ICP-MS for U—Pb analysis and selected trace elements, TE, (Ti, V, Cr, Fe, Zr, Nb, M, Sn, Sb, Hf, Ta, W, U) following the methodology outlined by Odlum and Stockli (2019). The trace element data were used to determine petrologic and tectonic affinity and crystallization temperatures of rutile. DR U—Pb results were binned into the same major groups as the DZ U—Pb data, and summarized in terms of percentages in Table 3 and as KDEs and histograms with a binwidth and bandwith of 20 in Fig. 9A, and petro-tectonic affinity and crystallization temperatures in Fig. 9B and tabulated in dataset S4 in the Supplementary material.

Potential source areas of detrital rutile U—Pb age components can be interpreted based on the known tectono-thermal history of the potential source terranes, especially major exhumation and/or metamorphic events. Additionally, the Zr-in-rutile thermometer and Cr/Nb felsic versus mafic classification can aid in differentiating source terranes based on the metamorphic grades and lithologies (Triebold et al., 2012). The main age components in the detrital rutile U—Pb ages in the Pyrenean realm are the same as the main zircon U—Pb age components. However, there are age components associated with Early Cretaceous and Jurassic thermal events recorded in the rutile U—Pb that are not recorded in zircon U—Pb ages

4. Source region isotopic signatures

Identifying sediment sources across the Pyrenean orogenic system requires the characterization of the various isotopic signatures preserved in the bedrock record. Here we describe the geochronology, thermochronology, and geochemistry for the diagnostic sedimentary sources and respective tectonic provinces. The sedimentary sources from youngest to oldest (shallow to deepest) include Mesozoic sedimentary cover rocks, the underlying Paleozoic sediment and metasedimentary units, and the Paleozoic-Neoproterozoic basement in the orogenic core.

Table 2
Detrital zircon (U—Th)/He results summarized in component percentages.

Sample	n	Pyrenean	Late Cretaceous	Early Cretaceous	Jurassic	Triassic-Paleozoic
		0–70 Ma	70–85 Ma	85–145 Ma	145–200 Ma	> 200 Ma
16-RB-02	16	0.0%	6.25%	50.0%	43.75%	0.0%
16-RB-03	16	0.0%	0.0%	43.75%	43.75%	12.5%
16-RB-05	13	30.8%	30.8%	38.4%	0.0%	0.0%
15-AB-164	13	69.2%	15.4%	15.4%	0.0%	0.0%
15-AB-162	21	38.1%	19.0%	33.3%	4.8%	4.8%
15-AB-161	20	60.0%	15.0%	20.0%	5.0%	0%
15-AB-163	21	19.0%	14.3%	28.6%	9.5%	28.6%
16-RB-12	13	100%	0.0%	0.0%	0.0%	0%
17-RB-14	12	100%	0.0%	0.0%	0.0%	0%

Table 3
Detrital rutile U−Pb Results summarized in component percentages.

Sample	Formation	n	Cretaceous	Post-Variscan	Variscan	Cambrian-Silurian	Cadomian	Neoproterozoic	Kibaran	Mesoproterozoic-Archean	Felsic	Mafic
			66–145 Ma	145–280 Ma	280–420 Ma	420–520 Ma	520–700 Ma	700–900 Ma	900–1200 Ma	> 1200 Ma		
15-AB-166	Adraén	29	0.0%	3.4%	20.7%	10.3%	34.5%	24.1%	6.9%	0.0%	79.3%	20.7%
16-RB-02	Late Cret.	20	0.0%	0.0%	15.0%	10.0%	40.0%	15.0%	5.0%	15.0%	52.4%	47.6%
16-RB-05	L. Corones	26	0.0%	7.7%	3.8%	0.0%	76.9%	7.7%	0.0%	3.8%	88.5%	23.1%
16-RB-06	U. Corones	37	2.7%	2.7%	13.5%	0.0%	59.5%	13.5%	2.7%	5.4%	89.2%	10.8%
15-AB-164	Campdevanol	39	0.0%	2.6%	23.1%	7.7%	41.0%	12.8%	2.6%	10.3%	62.5%	37.5%
16-RB-10	L. Milany	73	1.4%	1.4%	21.9%	12.3%	11.0%	13.7%	8.2%	30.1%	65.8%	34.2%
16-RB-14	Bellmunt	41	0.0%	0.0%	0.0%	0.0%	43.9%	9.8%	22.0%	24.4%	75.6%	24.4%

4.1. Mesozoic sedimentary sources

Upper-Permian to upper-Cretaceous strata represent an extensional basin system that likely formed a thick (up to ~6 km) sedimentary cover across significant proportion of the Axial Zone and thinned north to south across the NPZ, and SPZ structural provinces. Permian-Triassic sedimentary units are exposed along the southern and northern margin of the Axial Zone, and range in thickness laterally from tens of meters to kilometers. In the Southern Pyrenees, Permian-Triassic sedimentary strata is dominantly composed of red siltstones, sandstones, and conglomerates interbedded with minor volcanic rocks (Van Dongen, 1967; Gómez et al., 2004; Saura and Teixell, 2006). Previously published DZ U−Pb age distributions from an upper Permian sandstone from the southern Pyrenean Zone (i.e., Nogueres Zone) displays major peaks of Cambrian-Silurian (420–520 Ma) and Cadomian/Pan-African (520–700 Ma) ages with minor peaks of Carboniferous and Paleoproterozoic ages (Fig. 5C; SPZ-Nogueres Zone) (Whitchurch et al., 2011). The Permian-Triassic is overlain by thin Jurassic limestones and dolomites (Mey et al., 1968).

Cretaceous strata (Aptian to Coniacian) are found throughout the Pyrenees and were deposited during rifting and the opening of extensional or transtensional basins along the Iberian-European margin (Fig. 1; e.g., Vergés et al., 2002; Muñoz, 1992; Teixell et al., 2016). The syn- to post-rift strata in the southern Pyrenean basins are composed of shallow marine carbonates and marls, interbedded with clastic-rich carbonates to sandstones (e.g. Puigdefàbregas and Souquet, 1986; García Senz, 2002). The most significant extensional basins in the southeast Pyrenees are the Organyà and Pedraforca extensional basins, that have been subsequently inverted during the Pyrenean orogeny, and are now located in the South-Central Pyrenean Unit and Pedraforca thrust-belt salients (Puigdefàbregas and Souquet, 1986; Berástegui et al., 1990; Vergés et al., 2002). The Albian Camarade Formation in the NPZ has a dominant Cambrian-Silurian (420–520 Ma) age peak with secondary Cadomian/Pan-African (520–700 Ma) ages, which is interpreted to represent sediments derived from exhumed Paleozoic rocks along the present footwall of the North Pyrenean Frontal Thrust (Vacherat et al., 2017). In the South-Central Pyrenees, DZ U−Pb age distributions from Lower Cretaceous sedimentary units in the central Pyrenees yield a dominant Variscan age peak that is interpreted to represent southern basement extensional footwall areas as sediment sources for the Albian extensional basins (Fig. 5A) (Filleaudeau et al., 2011; Vacherat et al., 2017).

Characteristic thermochronometric cooling ages in the Mesozoic stratigraphy include Early Cretaceous ZHe ages (100–145 Ma) associated with the well-documented period of rifting-hyperextension and high-temperature metamorphism along the Iberian-European margin. The Early Cretaceous ages in the foreland basin are likely derived from recycling of Early Cretaceous syn-rift sedimentary units, presently exposed within the Pedraforca thrust sheet and inverted Organyà basin to the west. Additionally, Late Cretaceous ZHe ages (70–100 Ma) are interpreted to reflect earliest exhumation and cooling along the Iberia-European margin associated with initial convergence and structural inversion and are found in Paleozoic basement uplifts along the Agly and Salvezines Massifs and associated Mesozoic sedimentary cover units (Fig. 5B) (Ternois et al., 2019).

4.2. Paleozoic sedimentary and metasedimentary sources

The Paleozoic sedimentary sequences in the region consist of upper Neoproterozoic to middle Carboniferous sedimentary rocks and are present across the Eastern and Central Axial Zone in the Pyrenees and the southern Catalan Coastal Ranges (Margalef et al., 2016). The section can be divided into two major units: (1) the lower succession is dominantly metapelites and meta-arkose interbedded with marble, quartzite, calc-silicate and orthogneiss sheets. The syn-depositional meta-volcanic rocks yielded late Neoproterozoic–early Cambrian U−Pb ages (Fig. 5B) (575 ± 4 Ma in the Canigó massif, 558 ± 3 Ma in the Cap de Creus massif, LA-ICP-MS in zircon, Casas et al., 2015); and (2) the middle part of the succession is composed of Cambro to Ordovician low-grade metamorphosed sandstones and shales of the Júpols Group, Silurian black shales, Devonian limestones, and Carboniferous siliciclastic sedimentary units of the Culm Facies (Laumonier, 1988; Laumonier et al., 2010; Margalef et al., 2016). DZ U−Pb age distributions from the Cambro-Ordovician (Júpols Group) and Upper Ordovician strata in the eastern Pyrenees are characterized by predominantly Precambrian ages and contain dominate Cadomian/Pan-African (520–700 Ma), Kibaran (900–1200 Ma), Paleoproterozoic (1900–2100 Ma), and Neoarchean (2500–2650 Ma) age components (Fig. 5B), which are interpreted to have a Saharan Craton provenance along the northeast margin of Gondwana (Margalef et al., 2016).

Thermochronometric ages of the Paleozoic metasedimentary sequence include Late Triassic- Jurassic (200–145 Ma) cooling ages associated with rifting between the Alpine Tethys and the Central Atlantic oceans driving a regional-scale, Pyrenean-Alpine exhumation (Manatschal, 2004; Vacherat et al., 2016). Jurassic bedrock ZFT and ZHe ages (200–145 Ma) are found throughout the Catalan Coastal Ranges (Fig. 5B) and slightly younger Middle to Late Jurassic cooling ages (~180–150 Ma) have been documented in Corsica-Sardinia (Malusà et al., 2014, 2015; Vacherat et al., 2014). Therefore, potential source areas for these ages in the foreland deposits include recycling of Paleozoic metasedimentary units along the Axial Zone and Catalan Coastal Ranges (Fig. 5B), and/or sources to the east of the eastern Pyrenees (i.e., Corsica-Sardinia) that were subsequently rifted away in the Miocene (Gueguen et al., 1998; Roca et al., 1999; Séranne, 1999; Rosenbaum et al., 2002; Gunnell et al., 2008).

Triassic ZHe and ZFT ages are associated with a well-documented Triassic denudational event associated with extension of the Paleozoic crust (e.g. Vissers, 1992). Triassic and older ZHe ages can be from two possible sources: 1) recycling of sedimentary, most likely from Permian-Triassic sedimentary rocks, which is supported by the regional unconformity between Permian-Triassic sandstones and Variscan granites in some areas of the Axial Zone, or 2) from the south-southeast in the Catalan Coastal ranges where there are some in-situ bedrock Triassic ZFT ages (Fig. 5B) (Juez-Larré and Andriessen, 2006).

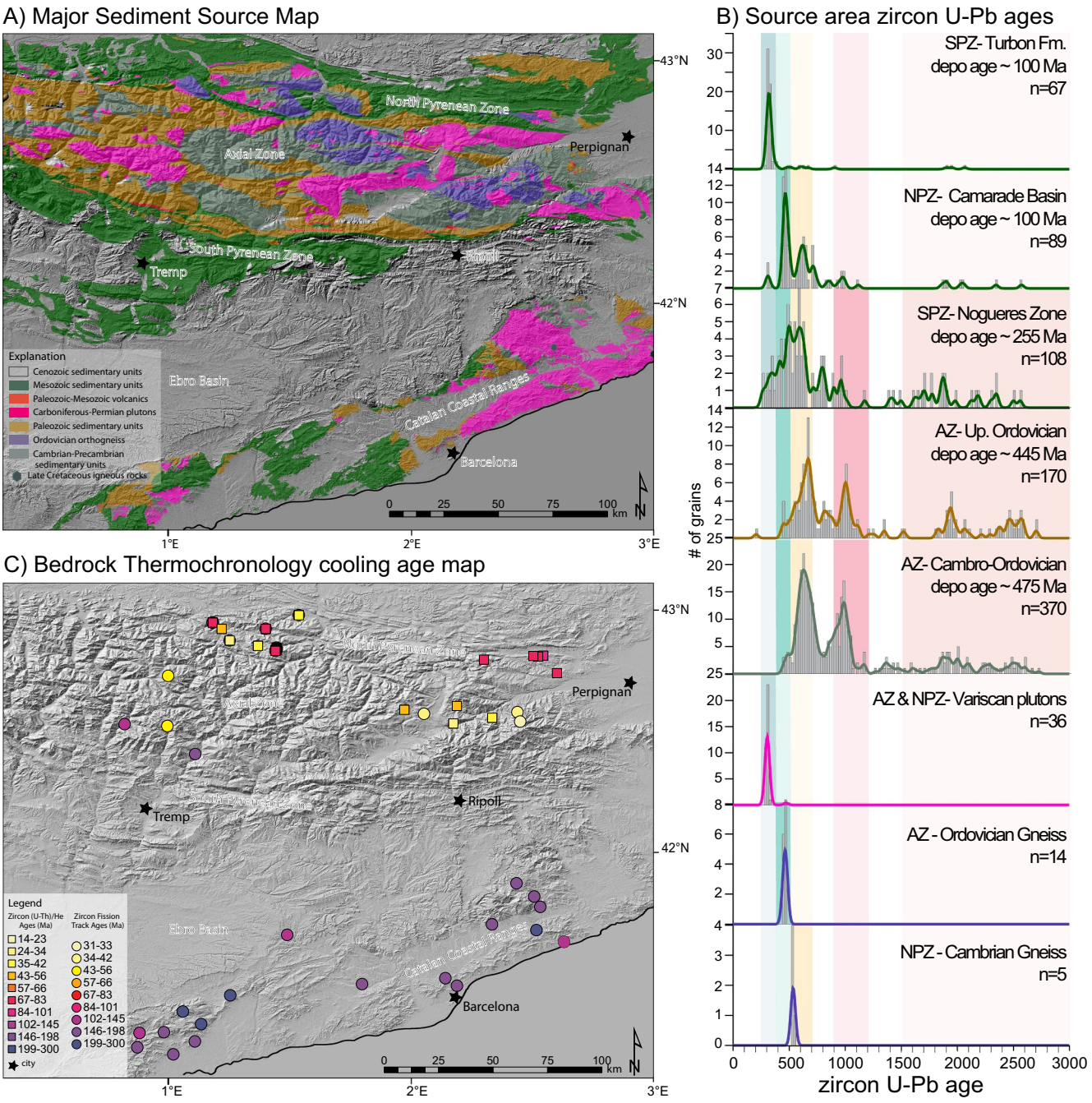

Fig. 5. Ripoll Basin sediment source area isotopic characterization bedrock maps and U—Pb zircon age data A) Geologic map of major sediment source lithologies in the eastern Pyrenees and northern Catalan Coastal Ranges. B) Source area zircon U—Pb age distributions from South Pyrenean Zone (SPZ), North Pyrenean Zone (NPZ), and Axial Zone (AZ) (data from Filleaudeau et al., 2011, Margalef et al., 2016, Whitchurch et al., 2011, Guille et al., 2018, and Vacherat et al., 2017). C) Bedrock ZFT and ZHe cooling age Map eastern Pyrenees and Catalan Coastal Ranges (data from Sinclair et al., 2005; Juez-Larré and Andriessen, 2006; Maurel et al., 2008; Vacherat et al., 2016; Ternois et al., 2019).

The lack of exposed bedrock with Neoproterozoic U—Pb rutile ages suggests any Neoproterozoic and older aged rutile must be recycled from Cambro-Ordovician and Upper Ordovician rocks with similar aged detrital zircons that outcrop throughout the Axial Zone (Margalef et al., 2016).

4.3. Paleozoic igneous-metamorphic sources

Paleozoic igneous-metamorphic basement units include Cambro-Ordovician gneisses and Carboniferous-Permian granitic plutons that make up an extensive area of the Axial Zone and eastern Catalan Coastal Ranges (purple and pink units, Fig. 5A). There are two significant pre-Variscan igneous magmatic events recorded in the Pyrenees: Ediacaran-early Cambrian intrusive and extrusive magmatism dated between 580 and 540 Ma (Castiñeiras et al., 2008 and references within; Guille et al., 2018) and Early Ordovician magmatism dated between 475 and 460 Ma (Castiñeiras et al., 2008 and references within). Rocks associated with these episodes of magmatism are found in the Eastern Pyrenees and the North Pyrenean Zone (purple units, Fig. 5A) (Vitrac-Michard and Allègre, 1975; Deloule et al., 2002; Cocherie et al., 2005; Castiñeiras et al., 2008; Denele et al., 2009; Guille et al., 2018). The bulk of magmatism within the region occurred

between 330 and 290 Ma during the Variscan orogeny, when felsic melts generated granitic plutons (Zr content ~129–350 ppm; Innocent et al., 1994) that have likely contributed significant proportions of detrital zircons in the subsequent Mesozoic rifting and Cenozoic Pyrenean orogeny. Only minor magmatism occurred during Early Cretaceous rifting in the Eastern Pyrenees and is dated between 104 and 95 Ma (Golberg et al., 1986; Henry et al., 1998). There is no magmatism/plutonism associated with the Pyrenean orogeny between the Late Cretaceous-Miocene recorded in the Pyrenean realm (Choukroune, 1989; Whitchurch et al., 2011 and references within).

Cenozoic ZHe cooling ages (< 70 Ma) record Pyrenean orogenic shortening and exhumation during collision between Iberia and Europe. Importantly such ages are restricted to the thermally reset Paleozoic igneous-metamorphic basement along the Axial and North Pyrenean Zone that were exhumed and cooled in response to the Pyrenean Orogeny (Fig. 5B) (e.g. Whitchurch et al., 2011; Filleaudeau et al., 2011; Bosch et al., 2016; Thomson et al., 2017). ZHe bedrock ages < 70 Ma indicate the Axial Zone basement (granitoids and gneisses) were buried and reheated (to near or above the ZHe and ZFT closure temperatures, ~180–250 °C) prior to the onset of the Pyrenean orogeny giving them Cenozoic ZHe and ZFT ages that record exhumation and erosion during Pyrenean orogenesis (e.g. Filleaudeau et al., 2011; Thomson et al., 2017).

There are diagnostic detrital rutile U—Pb thermochronometric ages of Triassic (~200 Ma) and Cretaceous (~100 Ma) age that are absent in DZ U—Pb components (Whitchurch et al., 2011; Filleaudeau et al., 2011; Fillon et al., 2013; Vacherat et al., 2017). The Triassic aged rutile is likely associated with a widespread doleritic event associated with the Central Atlantic Magmatic Province (Marzoli et al., 1999; Rossi et al., 2003; Vacherat et al., 2017). Cretaceous (~100 Ma) aged rutile are associated with Early Cretaceous rifting- hyperextension and exhumation of middle to lower crustal rutile-bearing rocks within the present-day North Pyrenean Zone, presently found in granulite facies gneisses in the NPZ basement massifs (Odlum and Stockli, 2019). Early Neoproterozoic to Ordovician rutile ages are likely derived from the Ordovician-Neoproterozoic orthogneisses in the eastern Pyrenees. However, some of these gneisses underwent metamorphism and migmatization associated with the Carboniferous Variscan orogeny that would have partially or fully reset the rutile U—Pb ages. Carboniferous-Permian rutile ages are likely derived from these migmatized early Paleozoic gneisses, metamorphic aureoles of the Variscan granites, and Paleozoic metasedimentary sequence that experienced peak temperatures > ~450–550 °C during the Variscan orogeny.

5. Provenance results and interpretations

Complementary detrital datasets from the southeastern Pyrenean foreland basin succession provide the unique opportunity to resolve

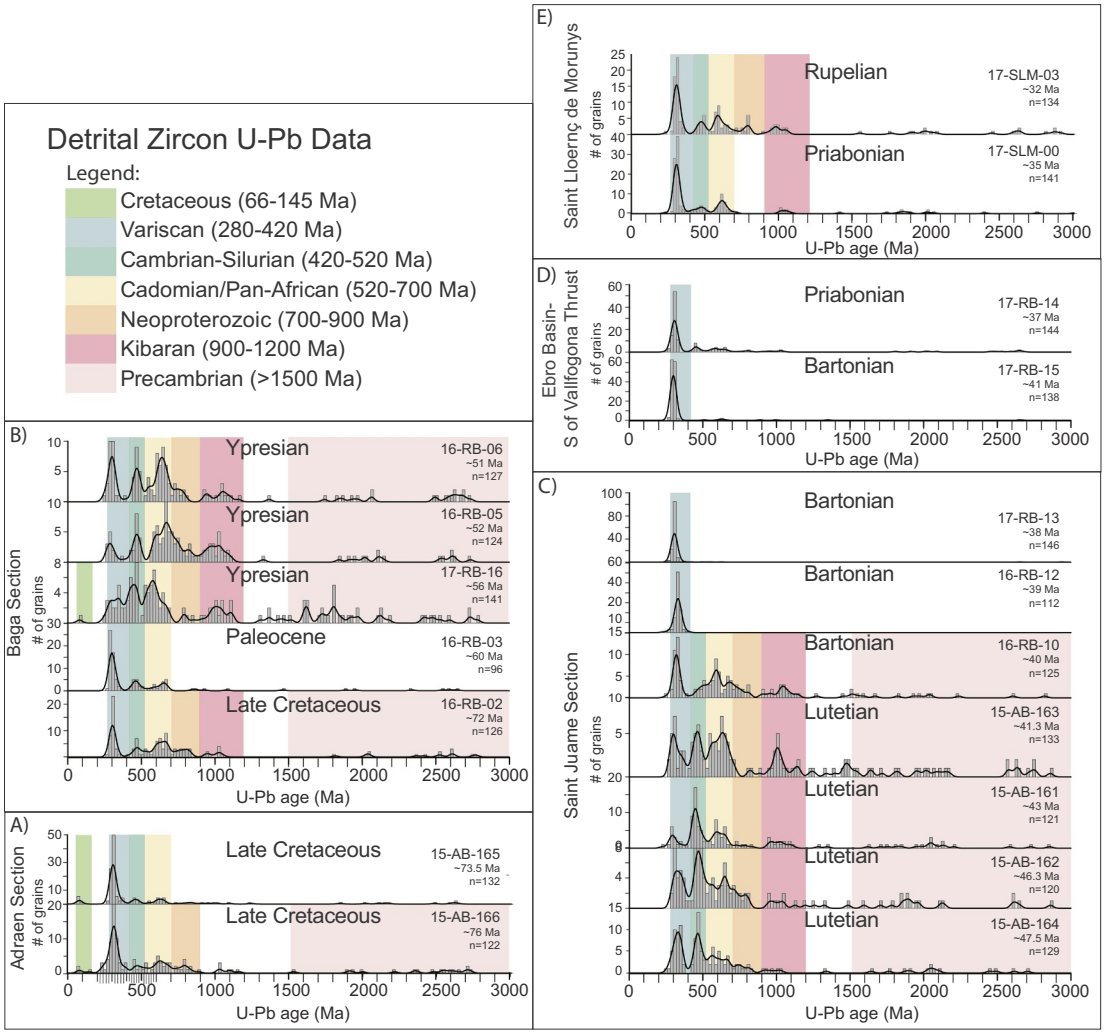

Fig. 6. Detrital zircon (DZ) U—Pb Kernel Density Estimator (KDE) plots organized by stratigraphic age. (A) Upper Cretaceous Adraén Section (B) Upper Cretaceous to Lower Eocene Bagà Section (C) Eocene Saint Juame Section (D) Upper Eocene Ebro Basin South of Vallfogona (E) Upper Eocene to Lower Oligocene Sant Llorenç de Morunys Section. Colored bars indicate main age components present in the samples.

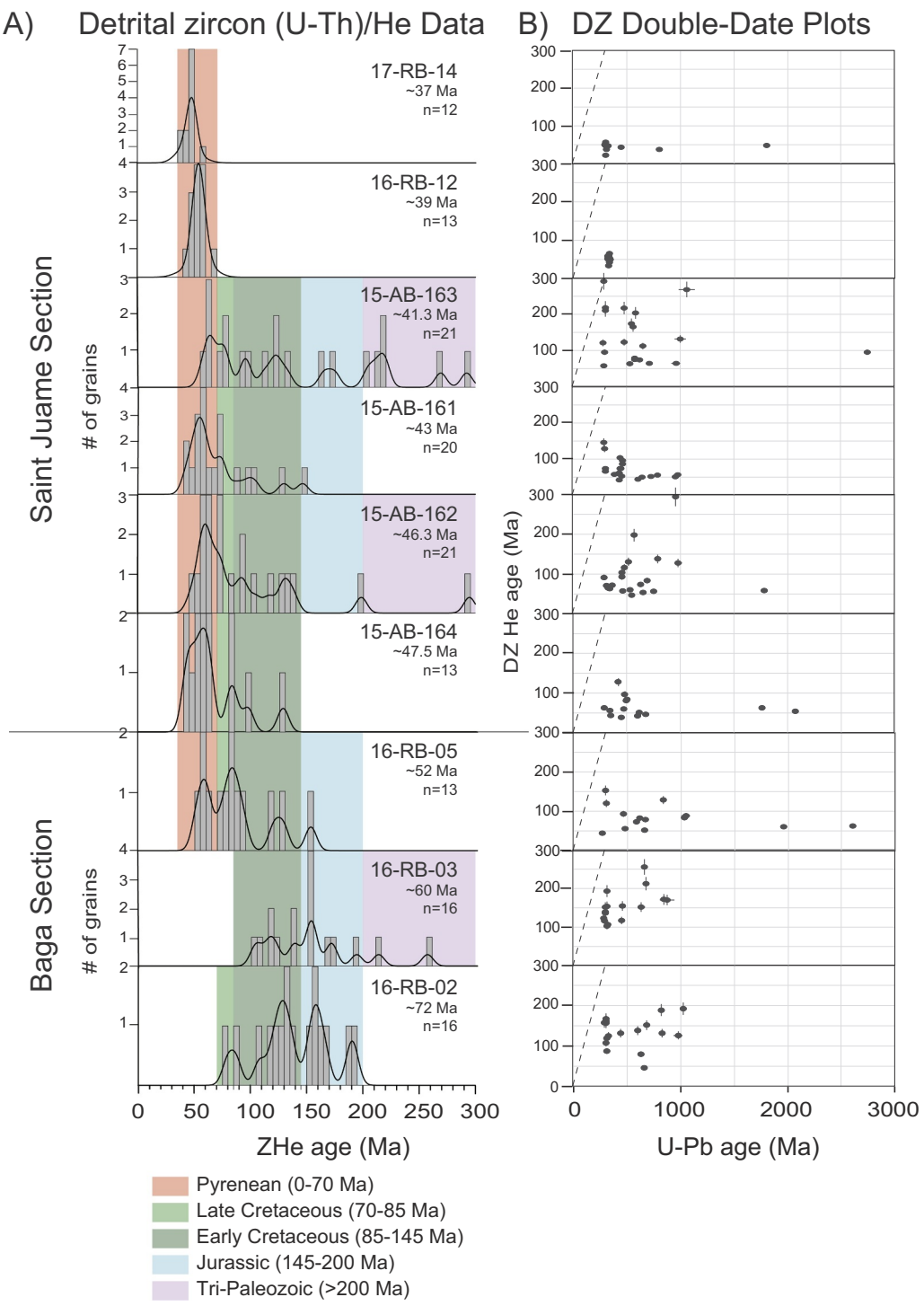

Fig. 7. Detrital zircon (U−Th)/He (ZHe) cooling age distributions and double-date time plots. A) ZHe Kernel Density Estimator (KDE) and histograms plots with a binwidth and bandwidth of 5 Ma, plotted from stratigraphically older to younger (bottom to top). Colored bars indicate main age components present in the samples. B) Double-date plots showing the U−Pb versus ZHe age of the detrital zircon grains, dashed line is the 1:1 age line.

lithospheric and Earth surface processes involved in the progressive closing and inversion of an extensional rift system along the Iberian and European plate margin. New geochronological (Fig. 6), thermochronological (Figs. 7, 8, 9A), and geochemical results (Fig. 9B) are grouped into six main phases (Fig. 10) based on stratigraphic and provenance trends observed in the Ripoll foreland basin to reconstruct provenance (Fig. 11) and compared with published shortening and exhumation trends in the hinterland and fold-thrust belt (Fig. 12). These six diagnostic stratigraphic intervals include (1) Late Cretaceous 80–66 Ma, (2) Paleocene 66–56 Ma, (3) Ypresian 56–47.8 Ma, (4)

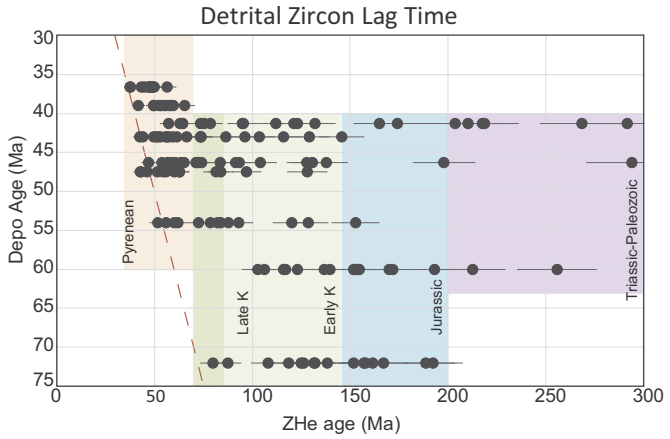

Fig. 8. Detrital zircon (DZ) Lag time plot between sample depositional age and DZ He cooling-ages (samples from Fig. 7). The colored bars indicate main age components present in samples. Dashed red line is the 1:1 age line. (For interpretation of the references to color in this figure legend, the reader is referred to the web version of this article.)

Lutetian 47.8–41.2 Ma, (5) Bartonian-mid-Priabonian 41.2–36 Ma, and (6) mid-Priabonian-mid-Oligocene 36–30 Ma (International Chronostratigraphic Chart v.2018) (Fig. 10).

5.1. Upper Cretaceous strata

5.1.1. DZ U–Pb and (U–Th)/He

The Adraén Formation (15-AB-166) has two Cretaceous aged grains that yield maximum depositional ages at 76.4 ± 4.8 Ma and 77.6 ± 5 Ma (Fig. 6). The DZ age spectrum has a dominant peak of Variscan (38% of all ages) with subordinate peaks of the other components (~3–15%). The Bona Formation (15-AB-165) has six Cretaceous grains ranging from 73.5 ± 3.7 to 81.6 ± 2.8 Ma. The maximum depositional age (MDA) calculated using the weighted mean average of the youngest 5 grains (overlapping within 2σ) is 76.2 ± 2.8 Ma, and from a single grain age is 73.5 ± 3.7. The age spectrum is dominated by Variscan aged grains (60%) with minor peaks of the other components (5–10%). The Maastrichtian sandstone in the Bagà section (sample 16-RB-02) has two dominant peaks of Variscan and Cadomian (~28%), with nearly equal components of Cambrian-Silurian, Neoproterozoic, Kibaran, and Mesoproterozoic and older (~10%). The Late Cretaceous sample from the Bagà section (16-RB-02) has ZHe ages that range from Late Cretaceous-Jurassic, with dominant components of Early Cretaceous (50%) and Jurassic (44%) ages (Fig. 7).

5.1.2. DR U–Pb and TE

The Adraèn Formation (15-AB-166) has mostly felsic affinity rutile (~79%), and a dominant Cadomian (35%) U–Pb age component, with secondary Neoproterozoic (~24%), and subordinate of Variscan, Cambrian-Silurian, and Kibaran (10–20%) rutile age components (Fig. 8). The Late Cretaceous sample from the Bagà section (sample 16-RB-02) is about half felsic (52%) and half mafic rutile (48%) and dominant Cadomian (40%) with subordinate Variscan, Cambrian-Silurian, Neoproterozoic, Kibaran, and Mesoproterozoic and older components (5–15%) (Fig. 9).

5.1.3. Interpretation

The Late Cretaceous samples from the Adraén section and Baga section (Fig. 3) are dominated by Variscan DZ U–Pb ages, and mostly felsic Cadomian and Variscan aged DR (Fig. 10). Upper Cretaceous shallow marine sandstone and carbonate strata of the Bagà section in the eastern Ripoll basin display similar DZ U–Pb Variscan dominated age spectra, with more Cadomian zircon ages, significantly more Cadomian DR ages and distinct rutile grains with mafic affinity which together are interpreted to represent sediment sources in the CCR and Corsica-Sardinia (Figs. 8, 11). Published petrographic compositions in the area contain abundant plutonic rock fragments, K-feldspar, quartz grains, and metamorphic rock fragments indicative of erosion of crystalline basement indicative of a basement sediment source along the northern CCR (Gómez-Gras et al., 2016). The Early Cretaceous and Jurassic ZHe ages are also indicative of sources in the CCR and Corsica-Sardinia (Fig. 5b; Malusà et al., 2015). Bedrock in-situ apatite fission track data and thermal modeling in the CCR support this interpretation and show that basement rocks of the CCR were near the surface (above the apatite partial annealing zone) forming a paleotopographic high during most of the Mesozoic (Juez-Larré and Andriessen, 2006). Additionally, Corsica-Sardinia preserve Early Cretaceous and Jurassic ZHe ages in Paleozoic basement rocks suggesting these rocks were also close to the surface and a potential major sediment source during the Late Cretaceous (Malusà et al., 2015 and references within).

The minor yet characteristic presence of Campanian aged zircons (~73–82 Ma) may also support a southern catchment area eroding Late Cretaceous igneous rocks from the Catalan Coastal Ranges (CCR), which has the only known Campanian aged igneous units presently outcropping in the region (Fig. 5A; Solé et al., 2003). These Late Cretaceous igneous units are alkaline and small/localized and therefore may not be the source of these zircons (due to small igneous rock volumes and assumed low zircon fertility), meaning these DZ were derived from some other Late Cretaceous igneous units in the region that have now been eroded away. Trace element analysis of the detrital zircon grains with Late Cretaceous ages predict a basaltic lithology (intermediate-mafic lithologies) using the classification and regression tree of Belousova et al., 2002(trace element data in S3), consistent with the lithologies in the CCR. However, there are abundant basaltic clasts in the Santonian-aged Campo Breccia (Mey et al., 1968) in the Tremp Basin to the west that may be sourced from local basaltic lithologies along the rift margin (present day Axial Zone) that have been eroded away. Detailed analysis and geochronology of the basalt clasts in the Campo Breccia are necessary to further investigate the possibility of local basalts in the Pyrenean realm (Cretaceous rift and post-rift) as a possible source of these DZ grains and differentiate between CCR and Pyrenean source area

The presence of Late Cretaceous ZHe ages in Late Cretaceous samples (Fig. 7) may suggest minor sediment contribution from sources within the Pyrenean realm, likely from recycling of syn-rift deposits near and overlying Paleozoic basement massifs in the earliest uplifting areas in the eastern NPZ (Fig. 5C; Ternois et al., 2019). Either scenario for the Late Cretaceous aged DZ grains (CCR or local Pyrenean basaltic sources) fits with the overall interpretation that the majority of the sediment was sourced from the east and southeast, with minor input from local sources in the Pyrenean realm (Fig. 11B).

5.2. Paleocene strata

5.2.1. DZ U–Pb and (U–Th)/He

The Paleocene sample from Bagà section (16-RB-03) has dominantly Variscan aged zircons (~53%) with minor components of Cambrian-Silurian and Cadomian components (~17% each) (Fig. 6). Detrital ZHe cooling ages are dominated by ZHe ages > 100 Ma with ~45% of Early Cretaceous and Jurassic components (Fig. 7). No rutile U–Pb and REE analysis were completed on the Paleocene section due to a lack of detrital rutile in the sample.

5.2.2. Interpretation

The Paleocene sample (16-RB-03) from the Bagà section has similar DZ U–Pb signatures to underlying upper Cretaceous strata, indicating no significant sediment provenance change (Figs. 6 and 10). The Paleocene Tremp Formation has a temporally condensed section consisting of poorly sorted, sandy to pebbly paleosols with barite nodules

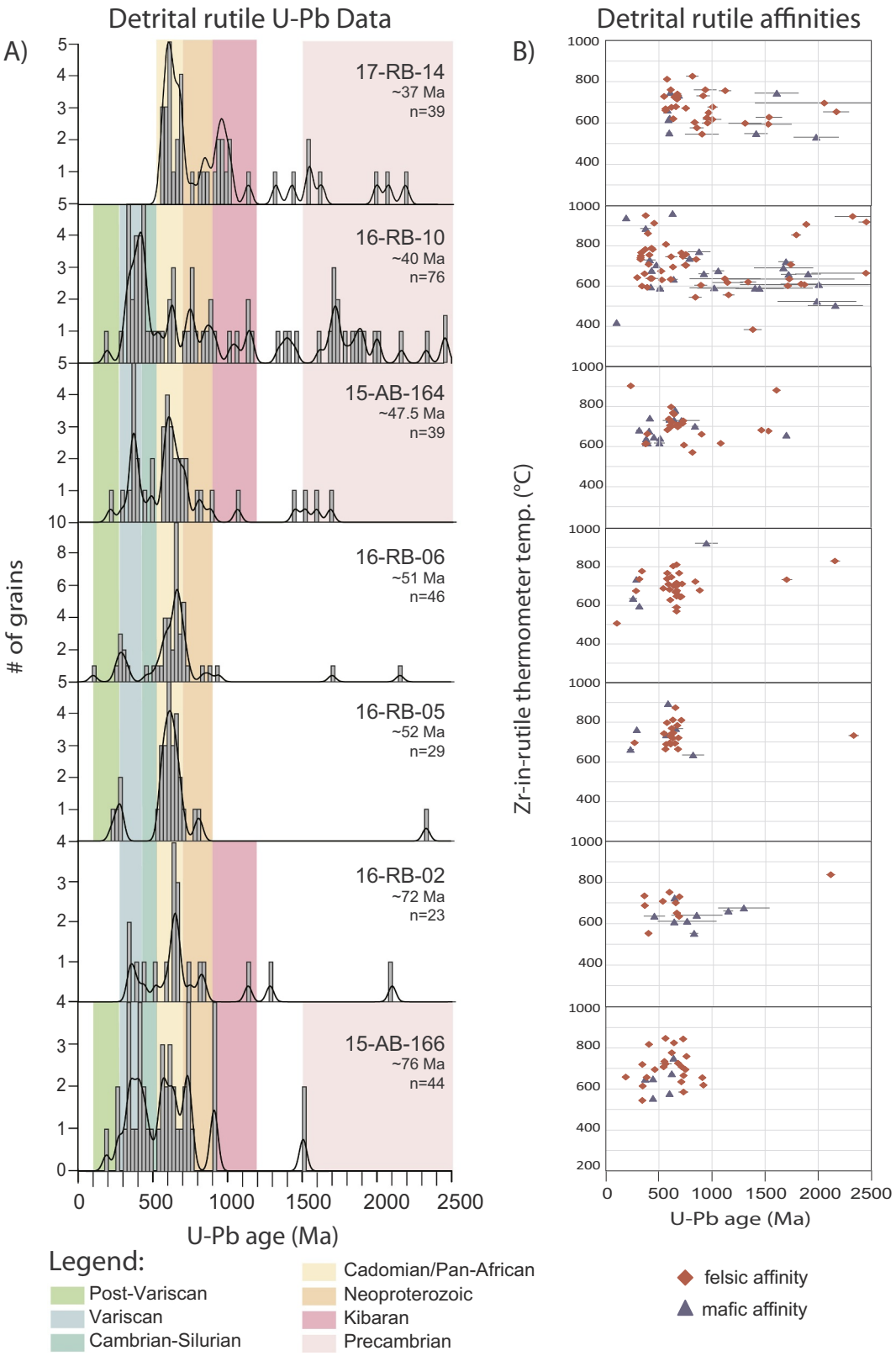

Fig. 9. Detrital rutile (DR) U–Pb age and geochemistry results. A) DR U–Pb age distributions Kernel Density Estimator (KDE) and histograms plots with a binwidth and bandwidth of 20 Ma, plotted from stratigraphically older to younger (bottom to top). Colored bars indicate main age components present. B) DR U–Pb age versus Zr-in-rutile calculated temperatures (Tomkins et al., 2007) and mafic or felsic affinities based on Cr and Nb classification of Triebold et al., 2012.

and fluvial fine to medium grained sandstones and has a DZ U–Pb signature dominated by Variscan U–Pb ages with Early Cretaceous-Triassic ZHe ages. This is consistent with continued sediment sources to the east and southeast in Corsica-Sardinia and the CCR (Fig. 11B). The lack of Late Cretaceous ZHe ages may reflect a cessation of sediment input from the NPZ during the phase of tectonic quiescence in the northern retro-wedge (Rosenbaum et al., 2002; Ford et al., 2016; Grool et al., 2018).

5.3. Early Eocene strata

5.3.1. Ypresian

5.3.1.1. DZ U–Pb and (U–Th)/He. The sample from the Sagnari marls (17-RB-16) age spectra differ significantly from older strata, with dominantly Mesoproterozoic and older grains (~30%) with a secondary peak of Cadomian zircons (~25%), and nearly equal components of Variscan, Cambrian-Silurian, and Kibaran (~14% each). Both samples from the Ypresian Corones Formation (16-RB-05 and 16-RB-06) have DZ age spectra with a dominant Cadomian component (28.0% and 31.5% respectively) and a cosmopolitan spectrum with presence of all (excluding post-Variscan) components between ~10–20%. Sample 16-RB-05 has dominantly Early Cretaceous and Late Cretaceous ZHe ages (~38%, 31% respectively) with the first appearance of Pyrenean ZHe ages (~31%).

5.3.1.2. DR U–Pb and TE. Both samples have mostly felsic rutile (~89% for both) with dominant peaks of Cadomian aged rutile (~80% and 60% respectively).

5.3.1.3. Interpretation. The Ypresian samples are characterized by multimodal DZ signatures (Fig. 6B), DR signature dominated by Cadomian ages (Fig. 9), and the first appearance of Cenozoic Pyrenean ZHe cooling ages (Fig. 7). The lowermost Eocene sample (17-RB-16) is from lacustrine marly sandstones in the Sagnari marls of the Cadi sequence (Puigdefàbregas et al., 1986; Burbank et al., 1992) (Fig. 3). The DZ U–Pb age spectra is multimodal, showing a decrease in the Variscan component and the appearance of the Kibaran and older age components. This age spectra, and the presence of Kibaran with older age components in both DR and DZ age spectra, are similar to the DZ U–Pb age spectra observed in late Paleozoic-Mesozoic sedimentary rocks (i.e. Permian-Triassic strata) and Paleozoic metasedimentary rocks in the Axial Zone indicating they became a significant sediment sources at this time (Figs. 5A, 11) (Margalef et al., 2016). The appearance of older DZ U–Pb and Pyrenean ZHe ages coincides with an observed basin deepening and changes from pedogenic to lacustrine carbonates and marls (Vergés et al., 1995; Burbank et al., 1992). The Mesozoic rift related strata, lower Cretaceous-Permian sedimentary rocks, are the first sediment sources from the north as unroofing in the Axial Zone (Fig. 11C). These contemporaneous changes in detrital signatures and stratigraphic architecture are interpreted as the onset of significant regional flexural subsidence and a change to a northern Pyrenean sediment source as the orogenic wedge began to deform and emerge (Fig. 11C). The Corones Formations DZ U–Pb age spectra are similar with presence of all the same U–Pb age components (except the disappearance of the minor Cretaceous age component) and an increase in the proportion of the Cambrian-Silurian and Cadomian age components compared to the underlying sample (17-RB-16) (Fig. 10). The proportion of Jurassic ZHe cooling ages decreases, compensated by the appearance and increase in the proportion of Pyrenean ZHe cooling ages compared to the Paleocene sample (Figs. 10, 12). The decrease in Variscan aged rutile is compensated by a dominance of Cadomian aged rutile with felsic affinities (Fig. 9). The changes in all provenance proxies from the Paleocene to the Early Eocene are interpreted to reflect an increased sediment supply from the growing Axial Zone to the north, specifically sediment derived from Mesozoic-Paleozoic sedimentary rocks (Early Cretaceous-Permian) and metasedimentary rocks (Cambrian-Ordovician) along with a decrease to cessation of sediment supplied from the east and southeast (Fig. 11C).

5.3.2. Lutetian

5.3.2.1. DZ U–Pb and (U–Th)/He. The Lutetian samples from the Sant Jaume section all show the presence of all the defined age components. The Campdevanol Formation and Coubet Formation have similar U–Pb age spectra with dominant components of Variscan, Cambrian-Silurian, and Cadomian (~25% each) and minor components of Neoproterozoic, Kibaran, and Mesoproterozoic and older components (5–15%) (Fig. 6C). The lower Bellmunt Formation(15-AB-161) is dominantly Cambrian-Silurian ages (~32%) and Cadomian ages (~23%) (Fig. 6C). The upper Bellmunt Formation(15-AB-163) has dominant components of Cadomian and Mesoproterozoic and older (~25% each), with nearly equal components of Variscan, Cambrian-Silurian, and Kibaran (~15%) (Fig. 6C). Detrital ZHe age distributions from the Campdevanol Formation (15-AB-164) has dominantly Pyrenean ZHe ages (~70%) with presence of both Early and Late Cretaceous ZHe ages (~15% each) (Fig. 7). The Coubet Formation (15-AB-162) has dominantly Pyrenean ZHe ages (38%) and Early Cretaceous (~34%) with a secondary component of Late Cretaceous (~19%), and minor presence of Jurassic and Triassic-Paleozoic components (~5%) (Fig. 7). The Lower Bellmunt Formation (15-AB-161) has a dominant component of Pyrenean ZHe ages (60%) with secondary components of Early Cretaceous (20%), Late Cretaceous (15%), and presence of Jurassic ZHe ages (5%) (Fig. 7). The Upper Bellmunt Formation (15-AB-163) has a more cosmopolitan age spectra with mostly Early Cretaceous Zhe ages (~30%) and similar proportions of every component (~10–20%) and overall older ages than the Lower Bellmunt Formation (Fig. 7).

5.3.2.2. DR U–Pb and TE. The Campdevanol Formation (15-AB-164) has ~60% felsic and ~40% mafic rutile with a dominant age component of Cadomian (41%) and Variscan rutile (23%) (Fig. 9).

5.3.2.3. Interpretation. The Lutetian Coubet, Campdevanol, and Bellmunt sequences have provenance signatures that record continued sediment sources from the Cambrian-Ordovician metasedimentary rocks in the uplifting Axial Zone as the proportion of Pyrenean ZHe age component increases (Fig. 6C). The Early and Late Cretaceous ZHe age component decreases, and the Jurassic ZHe age component is no longer present suggesting the input from eastern and southeastern sources (Corsica-Sardinia and CCR) is negligible or cut off (Fig. 10).

5.4. Bartonian-Priabonian strata

5.4.1. DZ U–Pb and (U–Th)/He

The lower Milany sequence (16-RB-10) has mostly Cadomian and Variscan DZ U–Pb ages (~30 and 25% respectively) with presence of all other components (~10% each). Two samples from the middle and upper Milany sequence (16-RB-12 and 17-RB-13) display unimodal Variscan age DZ U–Pb (~95% each) spectra (Fig. 6C). The Bartonian sample (17-RB-15) located south of the Vallfogona fault (Fig. 2), also has a unimodal peak of Variscan ages (~91%) (Fig. 6D). The Priabonian sample (17-RB-14) south of the Vallfogona fault (Fig. 2) has dominantly Variscan ages (57%), with nearly equal and minor components of Cambrian-Silurian, Cadomian, Mesoproterozoic and older (~5–14%) (Fig. 6D). Both upper Eocene samples (16-RB-12 and 17-RB-14) have 100% Pyrenean ZHe cooling ages, specifically Paleocene-Eocene ages (ranging from 37.3 Ma to 65.3 Ma) (Fig. 7).

5.4.2. DR U–Pb and TE

The Milany sequence (16-RB-10) has ~66% felsic and ~34% mafic rutile. All the age components are present with a dominant Mesoproterozoic and older component (~30%), a secondary Variscan component (~22%), and nearly equal amounts of Cambrian-Silurian, Neoproterozoic, and Kibaran (~10%), and a small presence of

Cretaceous and Post-Variscan (Fig. 9). The Bartonian sample from south of the Vallfogona frontal thrust has ~76% felsic and 24% mafic rutile, with a dominant component of Cadomian aged rutile (44%), a secondary peak of Mesoproterozoic and older (25%) with subordinate components of Neoproterozoic and Kibaran. There is no rutile younger than Cadomian (520–700 Ma) present.

5.4.3. Interpretation

The southward prograding alluvial conglomerates of the Milany Formation in the Ripoll Syncline and just south of the Vallfogona Thrust (Fig. 2) show a change from the multi-modal DZ U–Pb signatures (16-RB-10) to an unimodal DZ U–Pb peak of Variscan aged zircon, with unimodal peaks of Pyrenean ZHe ~50 Ma, concurrent with a decrease and disappearance of Variscan DR ages and increase in Kibaran and Precambrian DR ages (16-RB-12 and 16-RB-13) (Figs. 6, 7, 8, 10). This change occurs in the lower Milany formation above an unconformity (interpreted to be resultant from hinterland thrusting), and coincides with granitic-gneissic clasts becoming present and increasingly abundant in the conglomeratic facies upsection (Burbank et al., 1992). The unimodal provenance signals in DZ U–Pb and ZHe indicate the Carboniferous-early Permian plutons as the primary sediment source, pinpointing the exposure and timing of Axial Zone plutonic-gneissic basement erosion along the Eastern Pyrenees (Fig. 11D).

The predominance of Variscan aged zircon over Cambrian-Silurian and Cadomian ages, despite the Cambrian-Neoproterozoic gneisses also outcropping in the present eastern Axial Zone, can be interpreted as either 1) sediment provenance from hinterland-proximal basins are biased toward basement sources with higher zircon fertility in the Carboniferous-early Permian felsic igneous complexes (Capaldi et al., 2017) or 2) the Neoproterozoic-Silurian gneisses are at a deeper structural level and not yet exposed at the surface by the Oligocene. The former is supported by dissimilarity between DZ U–Pb signal that is dominated by Variscan ages from Carboniferous-Permian felsic plutons and the DR age distribution dominated by Cadomian age component and the lack of Variscan ages. The coupled DZ-DR record highlights that the Ripoll basin receives DR from Paleozoic gneissic and metasedimentary units, and a biased DZ signal from the Carboniferous-Permian intrusions with relatively high zircon fertility within the Axial Zone. This high zircon fertility is interpreted based on these DZ-DR relationships and supported by whole rock geochemistry of the plutons (Zr ppm = 129–350 ppm (Innocent et al., 1994) where zircon % by volume = 1.15 wt% Zr based on the equations of Malusà et al., 2016 after Dickinson, 2008). This exhibits the utility of using multiple provenance proxies that can provide important provenance information from both felsic and mafic lithologies.

5.5. Late Priabonian-Oligocene strata

5.5.1. DZ U–Pb

Both Priabonian-Oligocene samples from the Sant Llorenç de Morunys section (17-SLM-00 and 17-SLM-03) have dominant components of Variscan (54 and 34% respectively) with a secondary peak of Cadomian (~20% each), and presence ~10% of Cambrian-Silurian and Mesoproterozoic and older DZ U–Pb age components (Fig. 6D).

5.5.2. Interpretation

The upper Priabonian pre-growth strata contains dominantly Variscan DZ U–Pb signatures suggesting a continued sediment source from the Variscan granitic basement. The rejuvenation of Devonian and Cadomian U–Pb age components that increase in proportion upsection into the syn-growth strata is interpreted to reflect the progressive uplift and recycling foreland basin deposits in the hanging wall of the Vallfogona thrust (Fig. 11E). The lower erodibility of foreland deposits within wedge-top depocenters will yield recycled age signatures back into the foreland basin as the ramp-flat style deformation propagates toward the foreland (Capaldi et al., 2017). This interpretation is supported by the lack of late Eocene- to Oligocene-aged detrital zircon fission-track grain ages found in the Oligocene sedimentary units, indicative of recycling of sedimentary sources that contain older zircon cooling ages (Figs. 7, 10, 11E) (Whitchurch et al., 2011).

6. Eastern Pyrenees and foreland basin evolution

To establish a comprehensive view of the Eastern Pyrenean hinterland deformation, fold-and-thrust belt advance, sediment routing, and foreland basin evolution we compare new stratigraphic trends in sediment provenance and changes in sediment lag time (lag time = ZHe cooling age- sample depositional age; Garver et al., 1999) (Figs. 8, 10), with previously published fold-and-thrust belt activity and hinterland exhumation trends (Whitchurch et al., 2011 and refs within; Ternois et al., 2019), shortening rates (Grool et al., 2018), basin subsidence curves (Vergés et al., 1998), and global climate record (Zachos et al., 2008; Veizer and Prokoph, 2015) (Fig. 12).

6.1. Late Cretaceous-Paleocene tectonic inversion

During the Late Cretaceous, convergence between the Iberian and Eurasian plates was accommodated by reactivation and inversion along normal faults across the entire length of the previous hyperextended rift system as the distal exhumed mantle domain closed in the NPZ (Jammes et al., 2009; Lagabrielle et al., 2010; Mouthereau et al., 2014). Structural inversion and shortening were accommodated equally on both the upper European and lower Iberian plates with an overall shortening rate ~1 mm/year (e.g. Grool et al., 2018). Low-temperature thermochronological data records Late Cretaceous cooling in the upper plate within eastern NPZ massifs (Fig. 12; Ternois et al., 2019). Additionally, Late Cretaceous initial movement along Upper Pedraforca Thrust translated Jurassic to Lower Cretaceous rift deposits along Triassic evaporite decollements southward into the incipient foreland basin (Fig. 12; Vergés et al., 2002; Ramos et al., 2002). Structurally inverted extensional systems along eastern NPZ and/or Upper Pedraforca thrust sheet would have generated localized relief causing recycling of Mesozoic late syn to post-rift deposits into the southern prowedge foreland. Relatively short, ~8 Ma, minimum ZHe lag times calculated from the Late Cretaceous ZHe ages interpreted to be sourced from the northeast Pyrenees is consistent with the onset of orogenic exhumation in the eastern Pyrenees during this period (Fig. 9) (Ternois et al., 2019). The interpretation that these lag times are from zircon cooling ages in the Pyrenees and thus reflect the exhumation in the northeast Pyrenees and not the CCR is favored since there are no observed ZFT cooling ages in the CCR younger than ~100 Ma (Fig. 5B) (Juez-Larré and Andriessen, 2006). However, the only existing data for the CCR is ZFT ages, and ZHe data from the CCR would aid in confirming this interpretation. Though there is likely minor sediment input sourced from the north, provenance data along with published petrography show the dominant sediment source during the Late Cretaceous is from the east, Corsica-Sardinia, and southeast, Catalan Coastal Ranges (Fig. 11B) (Gómez-Gras et al., 2016; Vacherat et al., 2017). The average lag time from the sample is ~67 Myr suggesting slow exhumation to the east and southeast in the dominant sediment source regions. These trends show a continuation of sediment provenance from the south, consistent with interpretations for Albian strata in the central Pyrenees (Turbon Formation, Filleaudeau et al., 2011).

The Late Cretaceous provenance signatures shows that the inherited structures exert first-order control of deformation and inherited sediment routing systems persist and strongly influence the early syn-orogenic deposition. Local sources are controlled by inversion of normal faults creating local uplifts and recycling syn- to post rift sedimentary rocks, and dominant sediment routing systems are inherited from the precursor rift phase and persist through early margin inversion.

The Paleocene displays an increase in minimum lag time from ~8 m.y. in the Late Cretaceous to ~43 m.y. in the early Paleocene. This

Fig. 10. Compilation plots from Lower Cretaceous to Oligocene Ripoll Basin stratigraphic levels (Figs. 6, 7, and 8). A) Detrital zircon U–Pb age distributions B) Detrital zircon (U–Th)/He thermochronometric cooling age distribution C) Detrital Rutile U–Pb age distributions. The colored bars indicate main age components present in samples, see Figs. 6 and 7 for explanations.

significantly longer lag times can be due to a decrease in exhumation and erosion (e.g. Garver et al., 1999; Bernet et al., 2004) which is consistent with very slow tectonic driven subsidence of 0.05 mm/yr (Fig. 12; Vergés et al., 1998; Grool et al., 2018). The decrease in exhumation, erosion, and deposition during the Early Paleocene is also supported by the presence of paleosols with barite nodules, indicative of slow deposition (Kraus, 1999; Bréhéret and Brumsack, 2000). There was continued inversion along the Upper Pedraforca Thrust sheet, and low-temperature thermochronometric data shows exhumation in the northern region of the Axial Zone in the Querigut massif through the Paleocene (Fig. 12; Whitchurch et al., 2011 and references within).

During the early Paleocene, shortening rates in the Iberian plate decreased to ~0.4 mm/yr and ceased in the upper European plate and is evident by the lack of deposition across the northern retro-wedge foreland basin (Fig. 12; Ford et al., 2016; Grool et al., 2018). Rosenbaum et al. (2002) proposed a regionally extensive period of tectonic quiescence during the Paleocene in Iberia and Africa, they hypothesize the cessation of shortening along the Iberian-Eurasian plate boundary may be attributed to the initiation of Alpine exhumation at 65 Ma. There is no significant change in the sedimentary provenance during this period, with continued sediment sources to the east and southeast (Fig. 11B).

6.2. Early Eocene: Pyrenean orogenesis

6.2.1. Ypresian

There are significant changes in hinterland and fold-and-thrust belt deformation and subsidence and deposition in the foreland basin beginning in the Early Eocene (Vergés et al., 1995, 1998; Burbank et al., 1992). This is recorded by a significant change in provenance signals, from DZ U–Pb age distribution from dominantly Variscan age (280–420 Ma) S/SE source region in the Paleocene to multi-modal age distributions indicative of N/NE source regions in the Eocene (Fig. 11C), coincident with a shift from fluvial and paleosol to lacustrine facies of the Sagnari marls in the Cadi sequence. During the early Eocene, the shortening rate reaches a peak rate of ~4.5 mm/yr and the basin experienced increased subsidence and accommodation space generation marked by abrupt shift from shallow carbonates to deep-marine marly turbidites during the Ypresian (Figs. 3, 11; Grool et al., 2018; Puigdefàbregas et al., 1986; Burbank et al., 1992). Ypresian samples exhibit a characteristic first appearance of Pyrenean ZHe ages and short ZHe lag times that decrease to nearly 0 Myr, indicating onset

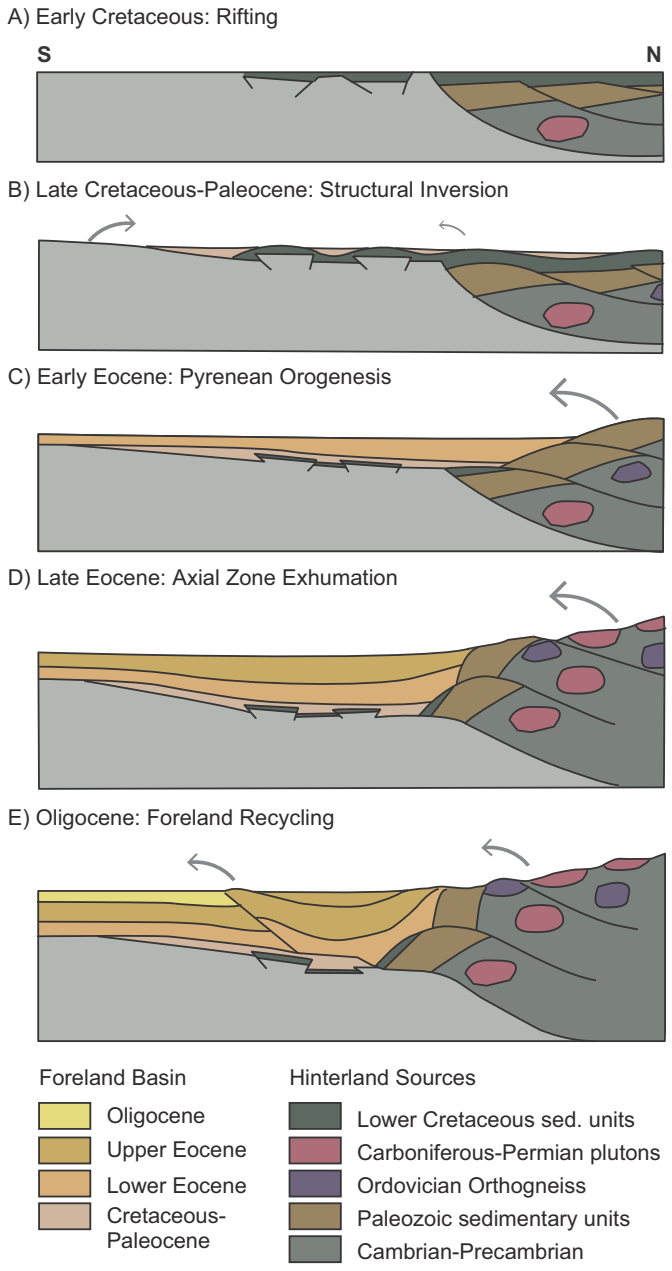

Fig. 11. Schematic cross sections demonstrating the Eastern Pyrenees foreland basin, hinterland exhumation and uplift, and sedimentary provenance evolution. Hinterland source colors correspond to map colors in Fig. 5A.

of accelerated exhumation and erosion in the NPZ and Axial Zone source areas (Fig. 11C) (Maurel et al., 2008; Metcalf et al., 2009; Beamud et al., 2011; Whitchurch et al., 2011; Filleaudeau et al., 2011; Vacherat et al., 2016; Ternois et al., 2019). The appearance of Pyrenean ZHe ages shows there was significant unroofing and exhumation, ~5–6 km, of the hinterland by this time (assuming a 35 °C/km geothermal gradient; Juez-Larré and Andriessen, 2006). The Corones Formation (depositional age ~ 51 Ma) deposits show the presence of a single Early Cretaceous aged (~100 Ma) rutile grain which definitively pinpoints the NPZ as a sediment source to the southern basin in the Early Eocene. This unique source identification places the paleo-drainage divide north of the north Pyrenean Fault during the Early Eocene for the eastern Pyrenees. This is similar to the provenance evolution in the Jaca Basin, the west-central pro-wedge foreland basin, where there were also sedimentary sources in the NPZ during the Eocene and subsequent southward drainage divide migration during the Eocene-Oligocene (Roigé et al., 2016).

6.2.2. Lutetian

The provenance trends in the Lutetian indicate progressive unroofing of the Axial Zone with cosmopolitan DZ, DR, and ZHe age spectra and the continued presence of Pyrenean ZHe ages and short lag times (Fig. 11C). The minor fluctuations in the Lutetian strata DZ and ZHe signals are likely associated with periods of Orri thrust sheet movement and Axial Zone exhumation (Figs. 6, 7, 11C). The west to southwest directed paleocurrents and hinterland unroofing trends in the basin reflects the progressive east to west exhumation in the Axial Zone (Sinclair et al., 2005; Whitchurch et al., 2011). There is an increase in the relative proportions of Variscan ages in DZ U—Pb and DR, and Pyrenean ZHe ages that may reflect increased basement input as the sedimentary cover (i.e., Early Cretaceous-Permian sedimentary units) is progressively eroded off the Axial Zone basement units (Fig. 10, 11C). Overall shortening rates decrease to ~2 mm/yr with deformation propagates into the foreland with development and motion along the Vallfogona Thrust (~44 Ma), driving subsidence further into the foreland (Jabalí subsidence curve, Figs. 2, 4, and 11) (Vergés et al., 1998). Exhumation of the Orri Basement thrust sheet is recorded by low-temperature thermochronometry (Fig. 12) (Grool et al., 2018; Fitzgerald et al., 1999; Metcalf et al., 2009; Whitchurch et al., 2011) and overall coarsening of grain sizes in the foreland basin (e.g. Burbank et al., 1992; Ramos et al., 2002).

A shorter, superimposed fluctuation in the overall unroofing trend occurs in the late Lutetian, with an increase in proportions of older components in DZ, ZHe, and DR signatures, as well as an increase in ZHe cooling age lag time (15-AB-164, 16-RB-10; Figs. 6, 8, 11). This increase in older DZ and DR age components implies that drainage catchments within the Axial Zone expanded with increased erosion and input of the Cambro-Ordovician metasedimentary units and Mesozoic sedimentary cover that contain these older age signatures (e.g. Whitchurch et al., 2011). The observed increase in lag time may be due to a decrease in exhumation related to the lower overall shortening rates in the orogen or due to the increased proportion of older, un-reset ZHe associated with the catchment expansion or a combination of both. Since there is a coeval increase in grain size in the foreland basin (Ramos et al., 2002) indicating sustained or increased exhumation in the hinterland, we favor the interpretation that there was catchment expansion (and no decrease in exhumation rates). This is also supported by the detrital signatures with the DZ U—Pb the DR U—Pb signatures becoming more multimodal as there are more varied sources in a larger catchment, and the DZ ZHe signature showing an increase in lag time associated with a more multimodal ZHe age spectra (samples 15-AB-163 (DZ) and 16-RB-10 (DR) (Figs. 6, 8)).

This observed fluctuation is contemporaneous with the Mid-Eocene Climatic Optimum (MECO) (Fig. 12; Zachos et al., 2008). Studies in the South-Central Pyrenean foreland basin have shown that climatic signal variation is well-preserved in the stratigraphy and are often the dominant forcing mechanism for the development of stratigraphic architecture (Dreyer and Fält, 1993; Ramos et al., 2002; Cantalejo and Pickering, 2015; Castelltort et al., 2017; Chen et al., 2018). These observations may suggest that there was a climate driven change in catchment area or erosion level during the MECO in the Eastern Pyrenees. Though this coincidence is intriguing and may have important implications for climate-tectonic interactions, additional work is needed to confirm that the increase in lag time and change in provenance signatures (more cosmopolitan spectra) is related to climatically driven changes in catchments and erosion during the MECO, and whether other climatic events show similar effects on provenance over the studied time period.

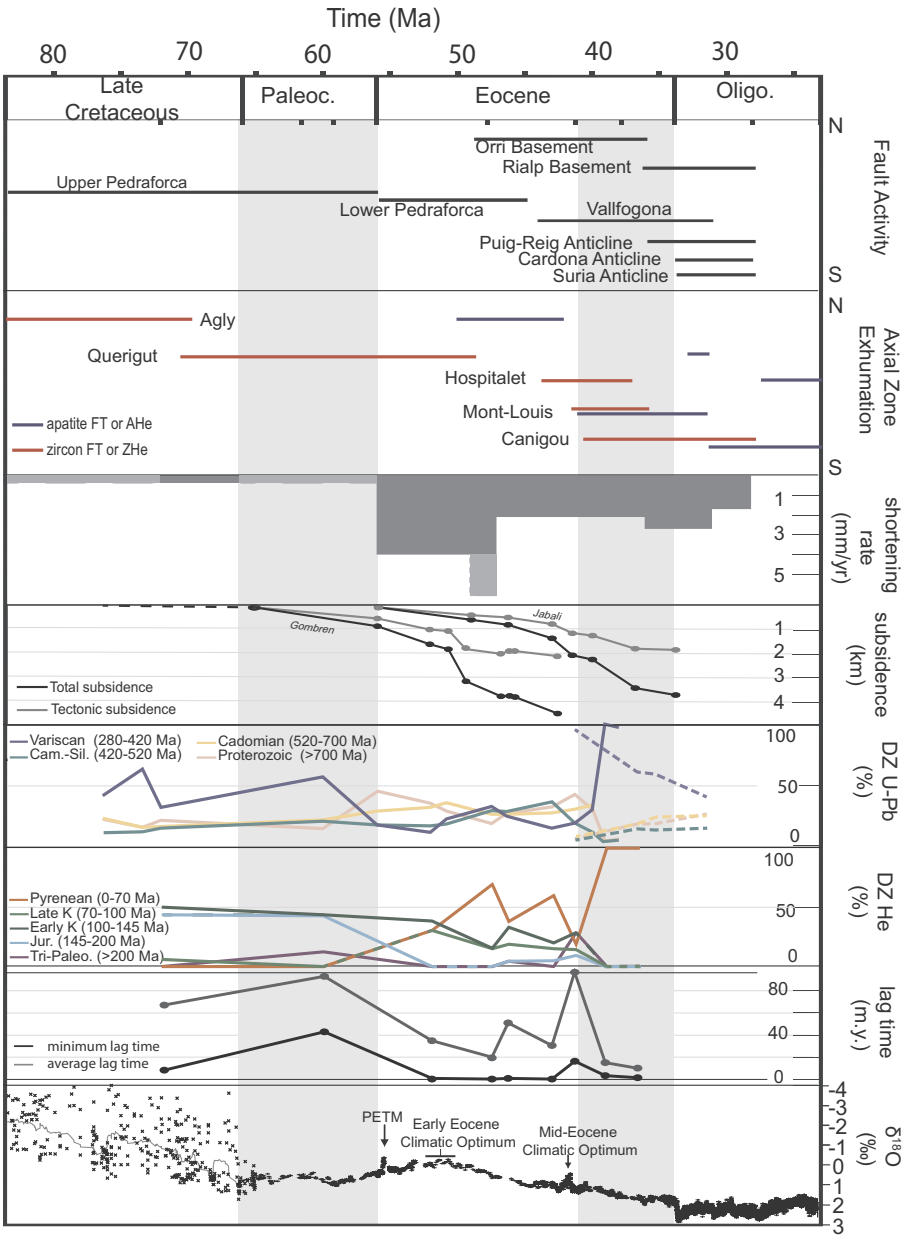

Fig. 12. Comparison among Eastern Pyrenees trends in hinterland exhumation, South Pyrenean zone fold-thrust belt deformation, Ripoll foreland basin subsidence, sedimentary provenance trends, and global $\delta^{18}O$ data during the Late Cretaceous to Oligocene. Lighter grey shortening rates have high uncertainty. Fault activity and shortening rates from Grool et al., 2018 and references within; Axial Zone exhumation from Whitchurch et al., 2011 and references within and Ternois et al., 2019; subsidence curves from the Gombren and Jabali sections of Vergés et al., 1998; $\delta^{18}O$ curve for the Cenozoic from Zachos et al., 2008 and for the Late Cretaceous from Veizer and Prokoph, 2015 and references within.

6.3. Late Eocene: Bartonian-Priabonian orogenesis

By the Mid to Late Eocene, DZ U−Pb and DZHe record unimodal Variscan crystallization ages (280–420 Ma) and Pyrenean (40–70 Ma) ZHe cooling ages, suggesting Carboniferous-late Permian plutons becoming the dominant source during a period of significant exhumation across Axial Zone massifs (Fig. 11D, 12; Vacherat et al., 2017). However, DR age distributions continue to record predominantly older > 520 Ma cooling ages indicative of Paleozoic metasedimentary source (Fig.9, Fig. 10). The discrepancy among the zircon and rutile provenance datasets (particularly sample 17-RB-14) highlights the zircon fertility bias within Variscan age igneous sources, and shows the utility of using multiple provenance proxies, especially between different mineral phases.

The timing of granitic-gneissic basement in the Eastern Pyrenees becoming a major sediment source is significantly later than previously estimated from provenance studies in the South-Central Pyrenees, where it is estimated to occur in the early Eocene (e.g. Filleaudeau et al., 2011; Whitchurch et al., 2011; Thomson et al., 2017). This is an important constraint on the Axial Zone evolution of the Eastern Pyrenees and illustrates the long-lived nature (~40 my) of recycling of Mesozoic syn-rift sedimentary cover and Paleozoic metasedimentary cover of the Axial Zone before granitic and gneissic basement were exposed and eroded (Fig. 11B–D).

6.4. Late Priabonian-Oligocene orogenesis and foreland recycling

The late Eocene to Oligocene samples in the Sant Llorenç de Morunys section are from pre-growth and syn-growth strata related to movement on the Vallfogona Thrust Fault (Riba, 1976; Ford et al., 1997; Suppe et al., 1997; Carrigan et al., 2016). The cannibalization of the early foreland basin deposits (Late Cretaceous-early Eocene strata) and recycling into Oligocene conglomerates is contemporaneous with an increase in shortening rates to ~3 mm/yr. The increase in shortening is mostly accommodated by ramp-flat style deformation propagating southward into the foreland leading to uplift and erosion in the wedgetop (Fig. 11E, 12).

7. Comparison with Tremp and Ager Basins

The DZ U—Pb provenance in the Eastern Pyrenees exhibit markedly different trends than in the central Pyrenees Tremp Basin (Whitchurch et al., 2011; Filleaudeau et al., 2011; Gómez-Gras et al., 2016; Clark et al., 2017). In the Maastrichtian, the Aren sandstone has dominant components of Cambrian-Silurian and Cadomian DZ U—Pb (Whitchurch et al., 2011), while the Eastern Pyrenees has dominantly Variscan DZ components. The two basins also show differences in sandstone composition based on petrography (Gómez-Gras et al., 2016). This could be attributed to isolated depocenters that are segmented by inherited structures, or dominance of local sediment sources in inverted isolated rift basins that have different petrographic and DZ U—Pb signatures. During the Paleocene, the U—Pb signatures between Tremp Formation samples are more similar, but with slightly different proportions of the Variscan, Cambrian-Silurian, and Cadomian components present (Whitchurch et al., 2011; Filleaudeau et al., 2011). However, in the upper Paleocene and lower Eocene, the DZ U—Pb signatures are starkly different between the two regions. The Roda sandstones in the Tremp Basin have a unimodal Variscan component, while the coeval Corones has multi-modal with the presence of Cambrian-Silurian, Cadomian, and Kibaran components. The Casstisent Formation in the Tremp Basin continues to be dominantly Variscan with minor presence of the older components (Whitchurch et al., 2011), and the coeval Campdevanol has nearly equal components of Variscan, Cambrian-Silurian, Cadomian DZ U—Pb ages. Additionally, the hypersaline conditions, poor faunal content, and evaporitic deposition during this period is strong evidence the Ripoll Basin was structurally partitioned from the Tremp basin to the west (Puigdefàbregas et al., 1986; Carrillo et al., 2014).

In the Mid-Eocene, the Montanyana Group in the Tremp Basin has presence of the Variscan, Cambrian-Silurian, Cadomian (Whitchurch et al., 2011) and the late Lutetian Escanilla Formation has a dominant Variscan component (Filleaudeau et al., 2011), while late Lutetian strata in the Eastern Pyrenees have multi-modal peaks and significant components of Cambrian-Silurian and older components (Fig. 6). However, the overlying Bartonian-Priabonian samples in the Eastern Pyrenees have unimodal peaks of Variscan DZ components, similar to the Escanilla Formation (Filleaudeau et al., 2011). In the late Priabonian to Oligocene, the Claramunt conglomerate in the Tremp Basin has multimodal age spectra with significant components of Variscan, Cambrian-Silurian, Cadomian, and some Neoproterozoic (Whitchurch et al., 2011), while in the Eastern Pyrenean Berga conglomerate is has a dominant Variscan component.

While the Tremp Basin shows different provenance signals than the Eastern Pyrenees, the Ager Basin shows a similar provenance evolution from the Late Cretaceous through the Eocene, with similar DZ U—Pb signatures and provenance interpretations (e.g. Whitchurch et al., 2011; Gómez-Gras et al., 2016; Clark et al., 2017; Thomson et al., 2019). The appearance of Cenozoic ZHe ages from the Axial Zone is coeval (Early Eocene) in both basins during deposition of the Corones Formation in the east and Baronia Formation in the Ager Basin. The similarity in provenance trends-signals suggests the two basins had similar basin evolution (i.e. foredeep to wedgetop) and sediment sources through time (i.e. CCR in the Late Cretaceous and Paleocene to eastern Pyrenean Axial Zone through the Eocene) (Whitchurch et al., 2011; Gómez-Gras et al., 2016; Clark et al., 2017; Thomson et al., 2019).

The differences in DZ provenance and sandstone composition signals between the Central Pyrenean Tremp Basin and the Eastern Pyrenean Ripoll basins can be accomplished by either multiple catchments feeding a single integrated basin or a broken foreland basin where the two basins were isolated through the entire Pyrenean orogeny (Gómez-Gras et al., 2016). We favor the interpretation of a broken foreland where the basins were partitioned by inherited rift features, specifically the Pedraforca unit, based on depositional/dispersal patterns, unique provenance signals (with no evidence of along axial mixing), facies suggesting restriction of the Ripoll Basin, and the inversion history of inherited structures (Fig. 12). This highlights the role of attenuated crust on foreland basin development, connectivity, and evolution, and the differences in attenuated-broken plate systems from the classic fold-and-thrust belt and foreland basin models built on uniform, rigid plates (e.g. DeCelles and Giles, 1996).

8. Implications for inverted rift orogens

The new constraints on the provenance coupled with the hinterland and fold-and-thrust belt evolution provides important constraints in the Eastern Pyrenees and highlights the dominant role of extensional inheritance on the evolution of the fold-and-thrust belt and foreland basins. The early inversion phase is characterized by early localized uplifts along inverted inherited normal faults across the margins, and in the eastern Iberian-European margin (Agly-Salvezines massifs; Ternois et al., 2019) where the inherited Early Cretaceous rift margin is been interpreted to have been the narrowest at the onset of convergence (Roca et al., 2011; Jammes et al., 2014; Ternois et al., 2019). The early syn-orogenic basins are likely segmented by the inherited rift system, as exemplified in the Pyrenees by the difference in provenance signatures between the Ripoll and Tremp Basins (Gómez-Gras et al., 2016; Clark et al., 2017). There is a dominance of inherited sediment routing systems, with sedimentary sources in the east and southeast (foreland/craton sources), that persists through the inversion phase and early synorogenic sedimentation. A new sediment routing system is established in the Early Eocene when the rift domain closed and antiformal stacking of basement thrust sheets began in the hinterland, ~25 m.y. after the onset of convergence, with hinterland sources becoming dominant. Inversion of pre-existing structures and basement involved thrusting in the hinterland accommodates shortening in the pro-wedge fold-and-thrust belt for ~35 m.y, until ramp-flat style shortening in the stratigraphic wedge begins (i.e. initiation of the Vallfogona Thrust) leading to recycling of earlier foreland basin deposits from the fold-and-thrust belt.

9. Conclusions

The South Eastern Pyrenean foreland basin is an ideal location to understand foreland basin and fold-thrust belt evolution superimposed over an inverted rift margin. Detrital zircon U—Pb, (U—Th)/He, and detrital rutile U—Pb and geochemistry are used to constrain the sediment provenance variations during Pyrenean exhumation and foreland basin evolution. (1) In the Late Cretaceous, the foreland basin depocenters are partitioned due to the inherited crustal architecture formed during Early Cretaceous rifting, with proximal flexure associated with localized structural inversion along inherited normal fault bounded rift basins. Distal southeastern and eastern sources located in the Catalan Coastal ranges and potentially from Corsica and Sardinia (prior to Miocene extension and translation into Mediterranean Sea) dominated the initial foreland basin until the early Eocene. Inherited drainage patterns established before the contractile phase continued for ~30 Myr after the onset of convergence. (2) The lower Eocene detrital zircon geo- and thermochronology reflects a shift to Pyrenean Axial Zone sediment sources as the catchment changed from east-southeast to the north in response to the enhanced uplift and erosion within the Pyrenean hinterland. (3) During the Eocene, detrital populations composed of Mesozoic sedimentary sources, Paleozoic metasedimentary rocks, and Carboniferous-early Permian plutonic rocks record a progressive tectonic unroofing into the Axial Zone. Additionally, there is a shift in one sample's DZ U—Pb age distributions and lag-times that coincides with the (Mid-Eocene Climate Optimum) MECO that may represent climate driven catchment expansion and enhanced erosion leading to increased exhumation of Carboniferous-early Permian plutonic rocks to the surface. (4) In the Late Eocene-Oligocene, recycling of earlier foreland basin deposits occurs as the fold-thrust belt continues to propagate toward the foreland. The new geochronological,

thermochronological, and geochemical dataset coupled with key stratigraphic changes highlight the relationships and feedbacks that exist among hinterland exhumation, fold-thrust belt evolution, foreland basin deposition and provenance in the Eastern Pyrenees which can be used to understand orogenic and foreland basin systems in other inverted rifts.

Supplementary data to this article can be found online at https://doi.org/10.1016/j.tecto.2019.05.008.

Acknowledgements

The authors would like to acknowledge the lifetime work of Josep Serra Kiel, whose research and scientific contributions in the Pyrenees has been fundamental to this work. We thank A. Teixell and A. Leier for constructive reviews that improved this manuscript. MLO and KDT are Equinor Fellows and thank Equinor Research Lab Austin for continuous support. This study was supported by 9GSA) Geological Society of America, United States, (AAPG) American Association of Petroleum Geologists, United States, and (SEPM) Society for Sedimentary Geology, United States student research grants awarded to MLO, and an Equinor grant to DFS. This manuscript greatly benefited from scientific discussion with B.K. Horton, S. Ternois, M. Curry, P. van der Beek, M. Roigé, D. Gómez-Gras, F. Mouthereau, F. Galster, L. Honegger, and S. Castelltort. The authors express gratitude to F. Galster, D. Patterson, L. Stockli for assistance with data collection, and A. Whitchurch for sharing analytical data. Sample locations and extended methodology can be found in the supporting information. Compiled U−Pb and (U−Th)/He data sets can be found as .xls files in the supporting information.

References

Babault, J., Teixell, A., Struth, L., Van Den Driessche, J., Arboleya, M.L., Tesón, E., 2013. Shortening, structural relief and drainage evolution in inverted rifts: insights from the Atlas Mountains, the Eastern Cordillera of Colombia and the Pyrenees. Geol. Soc. Lond., Spec. Publ. 377, 141–158.

Beamud, E., Muñoz, J.A., Fitzgerald, P.G., Baldwin, S.L., Garcés, M., Cabrera, L., Metcalf, J.R., 2011. Magnetostratigraphy and detrital apatite fission track thermochronology in syntectonic conglomerates: constraints on the exhumation of the South-Central Pyrenees. Basin Res. 23, 309–331.

Belousova, E., Griffin, W.L., O'Reilly, S.Y., Fisher, N.L., 2002. Igneous zircon: trace element composition as an indicator of source rock type. Contrib. Mineral. Petrol. 143 (5), 602–622.

Berástegui, X., Garcia-Senz, J.M., Losantos, M., 1990. Tecto-sedimentary evolution of the Organya extensional basin (central south Pyrenean unit, Spain) during the Lower Cretaceous. Bulletin de la Société Géologique de France VI, 251–264. https://doi.org/10.2113/gssgfbull.VI.2.251.

Bernet, M., Brandon, M.T., Garver, J.I., Molitor, B.R., 2004. Fundamentals of detrital zircon fission-track analysis for provenance and exhumation studies with examples from the European Alps. In: Special Paper 378: Detrital Thermochronology - Provenance Analysis, Exhumation, and Landscape Evolution of Mountain Belts. Geological Society of America, pp. 25–36. https://doi.org/10.1130/0-8137-2378-7.25.

Bosch, G.V., Teixell, A., Jolivet, M., Labaume, P., Stockli, D., Domenech, M., Monie, P., 2016. Timing of Eocene–Miocene thrust activity in the Western Axial Zone and Chaînons Béarnais (west-central Pyrenees) revealed by multi-method thermochronology. Comptes Rendus Géoscience 348 (3–4), 246–256.

Bréhéret, J.-G., Brumsack, H.-J., 2000. Barite concretions as evidence of pauses in sedimentation in the Marnes Bleues Formation of the Vocontian Basin (SE France). Sediment. Geol. 130, 205–228. https://doi.org/10.1016/S0037-0738(99)00112-8.

Burbank, D.W., Puigdefàbregas, C.A.I., Muñoz, J.A., 1992. The chronology of the Eocene tectonic and stratigraphic development of the eastern Pyrenean foreland basin, northeast Spain. Geol. Soc. Am. Bull. 104, 1101–1120.

Campbell, I.H., Reiners, P.W., Allen, C.M., Nicolescu, S., Upadhyay, R., 2005. He–Pb double dating of detrital zircons from the Ganges and Indus Rivers: implication for quantifying sediment recycling and provenance studies. Earth Planet. Sci. Lett. 237, 402–432.

Cantalejo, B., Pickering, K.T., 2015. Orbital forcing as principal driver for fine-grained deep-marine siliciclastic sedimentation, Middle-Eocene Ainsa Basin, Spanish Pyrenees. Palaeogeogr. Palaeoclimatol. Palaeoecol. 421, 24–47. https://doi.org/10.1016/j.palaeo.2015.01.008.

Capaldi, T.N., Horton, B.K., McKenzie, N.R., Stockli, D.F., Odlum, M.L., 2017. Sediment provenance in contractional orogens: the detrital zircon record from modern rivers in the Andean fold-thrust belt and foreland basin of western Argentina. Earth Planet. Sci. Lett. 479, 83–97.

Carrigan, J.H., Anastasio, D.J., Kodama, K.P., Parés, J.M., 2016. Fault-related fold kinematics recorded by terrestrial growth strata, Sant Llorenç de Morunys, Pyrenees Mountains, NE Spain. J. Struct. Geol. 91, 161–176. https://doi.org/10.1016/j.jsg.2016.09.003.

Carrillo, E., Rosell, L., Ortí, F., 2014. Multiepisodic evaporite sedimentation as an indicator of palaeogeographical evolution in foreland basins (South-eastern Pyrenean basin, Early-Middle Eocene). Sedimentology 61, 2086–2112. https://doi.org/10.1111/sed.12140.

Casas, J.M., Navidad, M., Castiñeiras, P., Liesa, M., Aguilar, C., Carreras, J., Hofmann, M., Gärtner, A., Linnemann, U., 2015. The Late Neoproterozoic magmatism in the Ediacaran series of the Eastern Pyrenees: new ages and isotope geochemistry. Int J Earth Sci (Geol Rundsch) 104, 909–925. https://doi.org/10.1007/s00531-014-1127-1.

Castelltort, S., Honegger, L., Adatte, T., Clark, J.D., Puigdefàbregas, C., Spangenberg, J.E., Dykstra, M.L., Fildani, A., 2017. Detecting eustatic and tectonic signals with carbon isotopes in deep-marine strata, Eocene Ainsa Basin, Spanish Pyrenees. Geology, G39068.1. https://doi.org/10.1130/G39068.1.

Castiñeiras, P., Navidad, M., Liesa, M., Carreras, J., Casas, J.M., 2008. U–Pb zircon ages (SHRIMP) for Cadomian and Early Ordovician magmatism in the Eastern Pyrenees: new insights into the pre-Variscan evolution of the northern Gondwana margin. Tectonophysics 461, 228–239.

Chen, C., Guerit, L., Foreman, B.Z., Hassenruck-Gudipati, H.J., Adatte, T., Honegger, L., Perret, M., Sluijs, A., Castelltort, S., 2018. Estimating regional flood discharge during Palaeocene-Eocene global warming. Sci. Rep. 8, 13391. https://doi.org/10.1038/s41598-018-31076-3.

Chevrot, S., Villaseñor, A., Sylvander, M., Benahmed, S., Beucler, E., Cougoulat, G., Delmas, P., de Saint Blanquat, M., Diaz, J., Gallart, J., Grimaud, F., Lagabrielle, Y., Manatschal, G., Mocquet, A., Pauchet, H., Paul, A., Péquegnat, C., Quillard, O., Roussel, S., Ruiz, M., Wolyniec, D., 2014. High-resolution imaging of the Pyrenees and Massif Central from the data of the PYROPE and IBERARRAY portable array deployments. Journal of Geophysical Research: Solid Earth 119, 6399–6420. https://doi.org/10.1002/2014JB010953.

Choukroune, P., the ECORS Team, 1989. The ECORS Pyrenean deep seismic profile reflection data and the overall structure of an orogenic belt. Tectonics 8, 23–39.

Clark, J.D., Puigdefabregas, C., Castelltort, S., Fildani, A., 2017. Propagation of Environmental Signals within Source-to-Sink Stratigraphy. In: SEPM Field trip Guidebook 13. SEPM (Society for Sedimentary Geology), Tulsa, OK.

Clerc, C., Lagabrielle, Y., Neumaier, M., Reynaud, J.-Y., Blanquat, M. de S., 2012. Exhumation of subcontinental mantle rocks: evidence from ultramafic-bearing clastic deposits nearby the Lherz peridotite body, French Pyrenees. Bulletin de la Société Géologique de France 183, 443–459. https://doi.org/10.2113/gssgfbull.183.5.443.

Cocherie, A., Baudin, T., Autran, A., Guerrot, C., Fanning, C.M., Laumonier, B., 2005. U-Pb zircon (ID-TIMS and SHRIMP) evidence for the early ordovician intrusion of metagranites in the late Proterozoic Canaveilles Group of the Pyrenees and the Montagne Noire (France). Bulletin de la Société géologique de France 176, 269–282.

Cowgill, E., Forte, A.M., Niemi, N., Avdeev, B., Tye, A., Trexler, C., Javakhishvili, Z., Elashvili, M., Godoladze, T., 2016. Relict basin closure and crustal shortening budgets during continental collision: an example from Caucasus sediment provenance. Tectonics 35, 2918–2947. https://doi.org/10.1002/2016TC004295.

Daignières, M., Séguret, M., Specht, M., Ecors Team, 1994. The Arzacq-western Pyrenees ECORS deep seismic profile. In: Hydrocarbon and Petroleum Geology of France. Springer, Berlin, Heidelberg, pp. 199–208.

Debroas, E.-J., 1987. Modèle de bassin triangulaire à l'intersection de décrochements divergents pour le fossé albo-cénomanien de la Ballongue (zone nord-pyrénéenne, France). Bulletin de la Société géologique de France 3, 887–898.

Debroas, E.-J., 1990. Le flysch noir albo-cénomanien témoin de la structuration albienne à sénonienne de la Zone nord-pyrénéenne en Bigorre (Hautes-Pyrénées, France). Bulletin de la Société géologique de France 6, 273–285.

DeCelles, P.G., Giles, K.A., 1996. Foreland basin systems. Basin Res. 8, 105–123.

Deloule, E., Alexandrov, P., Cheilletz, A., Laumonier, B., Barbey, P., 2002. In-situ U–Pb zircon ages for Early Ordovician magmatism in the eastern Pyrenees, France: the Canigou orthogneisses. Int. J. Earth Sci. 91, 398–405.

Denele, Y., Barbey, P., Deloule, E., Pelleter, E., Olivier, P., Gleizes, G., 2009. Middle Ordovician U-Pb age of the Aston and Hospitalet orthogneissic laccoliths: their role in the Variscan evolution of the Pyrenees. Bulletin de la Société Géologique de France 180, 209–216. https://doi.org/10.2113/gssgfbull.180.3.209.

Denèle, Y., Laumonier, B., Paquette, J.L., Olivier, P., Gleizes, G., Barbey, P., 2014. Timing of granite emplacement, crustal flow and gneiss dome formation in the Variscan segment of the Pyrenees. Geol. Soc. Lond., Spec. Publ. 405 (1), 265–287.

Dickinson, W.R., 2008. Impact of differential zircon fertility of granitoid basement rocks in North America on age populations of detrital zircons and implications for granite petrogenesis. Earth Planet. Sci. Lett. 275 (1–2), 80–92.

Dreyer, T., Fält, L.M., 1993. Facies analysis and high-resolution sequence stratigraphy of the Lower Eocene shallow marine Ametlla Formation, Spanish Pyrenees. Sedimentology 40, 667–697.

Fildani, A., Hessler, A.M., 2005. Stratigraphic record across a retroarc basin inversion: Rocas Verdes–Magallanes Basin, Patagonian Andes, Chile. Geol. Soc. Am. Bull. 117, 1596. https://doi.org/10.1130/B25708.1.

Filleaudeau, P.-Y., Mouthereau, F., Pik, R., 2011. Thermo-tectonic evolution of the south-central Pyrenees from rifting to orogeny: insights from detrital zircon U/Pb and (U-Th)/He thermochronometry. Basin Res. 24, 401–417. https://doi.org/10.1111/j.1365-2117.2011.00535.x.

Fillon, C., Gautheron, C., van der Beek, P., 2013. Oligocene–Miocene burial and exhumation of the Southern Pyrenean foreland quantified by low-temperature thermochronology. J. Geol. Soc. 170, 67–77.

Fitzgerald, P.G., Muñoz, J.A., Coney, P.J., Baldwin, S.L., 1999. Asymmetric exhumation across the Pyrenean orogen: implications for the tectonic evolution of a collisional

orogen. Earth Planet. Sci. Lett. 173, 157–170.
Ford, M., Williams, E.A., Artoni, A., Vergés, J., Hardy, S., 1997. Progressive evolution of a fault-related fold pair from growth strata geometries, Sant Llorenç de Morunys, SE Pyrenees. Journal of Structural Geology. Fault-Related Folding 19, 413–441. https://doi.org/10.1016/S0191-8141(96)00116-2.
Ford, M., Hemmer, L., Vacherat, A., Gallagher, K., Christophoul, F., 2016. Retro-wedge foreland basin evolution along the ECORS line, eastern Pyrenees, France. J. Geol. Soc. 173, 419–437.
Fosdick, J.C., Graham, S.A., Hilley, G.E., 2014. Influence of attenuated lithosphere and sediment loading on flexure of the deep-water Magallanes retroarc foreland basin, Southern Andes. Tectonics 33, 2505–2525. https://doi.org/10.1002/2014TC003684.
García Senz, J., 2002. Cuencas extensivas del Cretácico Inferior en los Pirineos centrales. Formación y subsecuente inversión. PhD Dissertation. Universitat de Barcelona.
Garver, J.I., Brandon, M.T., Roden-Tice, M., Kamp, P.J., 1999. Exhumation history of orogenic highlands determined by detrital fission-track thermochronology. Geol. Soc. Lond., Spec. Publ. 154, 283–304.
Gehrels, G., 2012. Detrital Zircon U-Pb Geochronology: Current Methods and New Opportunities. In: Tectonics of Sedimentary Basins. John Wiley & Sons, Ltd, pp. 45–62. https://doi.org/10.1002/9781444347166.ch2.
Gleizes, G., Leblanc, D., Bouchez, J.L., 1997. Variscan granites of the Pyrenees revisited: their role as syntectonic markers of the orogen. Terra Nova 9 (1), 38–41.
Golberg, J.M., Maluski, H., Leyreloup, A.F., 1986. Petrological and age relationship between emplacement of magmatic breccia, alkaline magmatism, and static metamorphism in the North Pyrenean Zone. Tectonophysics 129, 275–290.
Gómez, J.L., Marzo, M., Hernández, H.M.V., 2004. The siliciclastic Permian-Triassic deposits in Central and Northeastern Iberian Peninsula (Iberian, Ebro and Catalan Basins): a proposal for correlation. Geol. Acta 2, 305.
Gómez-Gras, D., Roigé, M., Fondevilla, V., Oms, O., Boya, S., Remacha, E., 2016. Provenance constraints on the Tremp Formation paleogeography (southern Pyrenees): Ebro Massif VS Pyrenees sources. Cretac. Res. 57, 414–427. https://doi.org/10.1016/j.cretres.2015.09.010.
Gómez-Paccard, M., López-Blanco, M., Costa, E., Garcés, M., Beamud, E., Larrasoaña, J.C., 2012. Tectonic and climatic controls on the sequential arrangement of an alluvial fan/fan-delta complex (Montserrat, Eocene, Ebro Basin, NE Spain). Basin Res. 24, 437–455. https://doi.org/10.1111/j.1365-2117.2011.00532.x.
Grool, A.R., Ford, M., Vergés, J., Huismans, R.S., Christophoul, F., Dielforder, A., 2018. Insights into the crustal-scale dynamics of a doubly vergent orogen from a quantitative analysis of its forelands: a case study of the Eastern Pyrenees: Insights into the crustal-scale dynamics of a doubly vergent orogen from a quantitative analysis of its forelands: a case study of the Eastern Pyrenee. Tectonics. https://doi.org/10.1002/2017TC004731.
Gueguen, E., Doglioni, C., Fernandez, M., 1998. On the post-25 Ma geodynamic evolution of the western Mediterranean. Tectonophysics 298, 259–269. https://doi.org/10.1016/S0040-1951(98)00189-9.
Guenthner, W.R., Reiners, P.W., Ketcham, R.A., Nasdala, L., Giester, G., 2013. Helium diffusion in natural zircon: Radiation damage, anisotropy, and the interpretation of zircon (U-Th)/He thermochronology. Am. J. Sci. 313, 145–198. https://doi.org/10.2475/03.2013.01.
Guille, B.T., Olivier, P., Paquette, J.-L., Bossé, V., Guillaume, D., 2018. Evolution of the middle crust of the Pyrenees during the Paleozoic: new data on the plutonic rocks from the North Pyrenean Agly Massif. Int. J. Earth Sci. 1–21.
Gunnell, Y., Zeyen, H., Calvet, M., 2008. Geophysical evidence of a missing lithospheric root beneath the Eastern Pyrenees: consequences for post-orogenic uplift and associated geomorphic signatures. Earth Planet. Sci. Lett. 276, 302–313. https://doi.org/10.1016/j.epsl.2008.09.031.
Gunnell, Y., Calvet, M., Brichau, S., Carter, A., Aguilar, J.-P., Zeyen, H., 2009. Low long-term erosion rates in high-energy mountain belts: insights from thermo- and biochronology in the Eastern Pyrenees. Earth Planet. Sci. Lett. 278, 208–218. https://doi.org/10.1016/j.epsl.2008.12.004.
Hart, N.R., Stockli, D.F., Hayman, N.W., 2016. Provenance evolution during progressive rifting and hyperextension using bedrock and detrital zircon U-Pb geochronology, Mauléon Basin, western Pyrenees. Geosphere 12, 1166–1186.
Hart, N.R., Stockli, D.F., Lavier, L.L., Hayman, N.W., 2017. Thermal evolution of a hyperextended rift basin, Mauléon Basin, western Pyrenees. Tectonics, 2016TC004365. https://doi.org/10.1002/2016TC004365.
Henry, P., Azambre, B., Montigny, R., Rossy, M., Stevenson, R.K., 1998. Late mantle evolution of the Pyrenean sub-continental lithospheric mantle in the light of new 40Ar–39Ar and Sm–Nd ages on pyroxenites and peridotites (Pyrenees, France). Tectonophysics 296, 103–123.
Horton, B.K., Saylor, J.E., Nie, J., Mora, A., Parra, M., Reyes-Harker, A., Stockli, D.F., 2010. Linking sedimentation in the northern Andes to basement configuration, Mesozoic extension, and Cenozoic shortening: evidence from detrital zircon U-Pb ages, Eastern Cordillera, Colombia. Bulletin 122 (9–10), 1423–1442.
Hourigan, J. K., Reiners, P. W., & Brandon, M. T. (2005). U-Th zonation-dependent alpha-ejection in (U-Th)/He chronometry. Geochimica et Cosmochimica Acta, 69(13), 3349-3365.
Innocent, C., Briqueu, L., Cabanis, B., 1994. Sr-Nd isotope and trace-element geochemistry of late Variscan volcanism in the Pyrenees: magmatism in post-orogenic extension? Tectonophysics 238 (1–4), 161–181.
Jammes, S., Manatschal, G., Lavier, L., Masini, E., 2009. Tectonosedimentary evolution related to extreme crustal thinning ahead of a propagating ocean: example of the western Pyrenees. Tectonics 28. https://doi.org/10.1029/2008TC002406.
Jammes, S., Huismans, R.S., Muñoz, J.A., 2014. Lateral variation in structural style of mountain building: controls of rheological and rift inheritance. Terra Nova 26, 201–207. https://doi.org/10.1111/ter.12087.
Juez-Larré, J., Andriessen, P.A.M., 2006. Tectonothermal evolution of the northeastern margin of Iberia since the break-up of Pangea to present, revealed by low-temperature fission-track and (U–Th)/He thermochronology: a case history of the Catalan Coastal Ranges. Earth Planet. Sci. Lett. 243, 159–180. https://doi.org/10.1016/j.epsl.2005.12.026.
Kooijman, E., Mezger, K., Berndt, J., 2010. Constraints on the U–Pb systematics of metamorphic rutile from in situ LA-ICP-MS analysis. Earth Planet. Sci. Lett. 293, 321–330. https://doi.org/10.1016/j.epsl.2010.02.047.
Kraus, M.J., 1999. Paleosols in clastic sedimentary rocks: their geologic applications. Earth Sci. Rev. 47, 41–70. https://doi.org/10.1016/S0012-8252(99)00026-4.
Lacombe, O., Mouthereau, F., 2002. Basement-involved shortening and deep detachment tectonics in forelands of orogens: Insights from recent collision belts (Taiwan, Western Alps, Pyrenees). Tectonics 21https://doi.org/10.1029/2001TC901018. (12-1–12-22).
Lagabrielle, Y., Bodinier, J.-L., 2008. Submarine reworking of exhumed subcontinental mantle rocks: field evidence from the Lherz peridotites, French Pyrenees. Terra Nova 20, 11–21. https://doi.org/10.1111/j.1365-3121.2007.00781.x.
Lagabrielle, Y., Labaume, P., Blanquat, M. de S., 2010. Mantle exhumation, crustal denudation, and gravity tectonics during Cretaceous rifting in the Pyrenean realm (SW Europe): insights from the geological setting of the lherzolite bodies. Tectonics 29. https://doi.org/10.1029/2009TC002588.
Laumonier, B., 1988. Les groupes de Canaveilles et de Jujols ("Paléozoïque inférieur") des Pyrénées orientales. Arguments en faveur de l'âge essentiellement cambrien de ces séries. Hercynica 4, 25–38.
Laumonier, B., Marignac, C., Kister, P., 2010. Polymétamorphisme et évolution crustale dans les Pyrénées orientales pendant l'orogenèse varisque au Carbonifère supérieur. Bulletin de la Société géologique de France 181, 411–428.
López-Blanco, M., Marzo, M., Burbank, D.W., Vergés, J., Roca, E., Anadoàn, P., Pina, J., 2000. Tectonic and climatic controls on the development of foreland fan deltas: Montserrat and Sant Llorencé del Munt systems (Middle Eocene, Ebro Basin, NE Spain). Sediment. Geol. 23.
Malusà, M.G., Danišík, M., Kuhlemann, J., 2014. Thermochronological response to rifting and subduction in the Corsica-Sardinia block. In: Presented at the EGU General Assembly Conference Abstracts, pp. 9676.
Malusà, M.G., Faccenna, C., Baldwin, S.L., Fitzgerald, P.G., Rossetti, F., Balestrieri, M.L., Danišík, M., Ellero, A., Ottria, G., Piromallo, C., 2015. Contrasting styles of (U)HP rock exhumation along the Cenozoic Adria-Europe plate boundary (Western Alps, Calabria, Corsica). Geochem. Geophys. Geosyst. 16, 1786–1824. https://doi.org/10.1002/2015GC005767.
Malusà, M.G., Resentini, A., Garzanti, E., 2016. Hydraulic sorting and mineral fertility bias in detrital geochronology. Gondwana Res. 31, 1–19.
Manatschal, G., 2004. New models for evolution of magma-poor rifted margins based on a review of data and concepts from West Iberia and the Alps. Int J Earth Sci (Geol Rundsch) 93, 432–466. https://doi.org/10.1007/s00531-004-0394-7.
Margalef, A., Castiñeiras, P., Casas, J.M., Navidad, M., Liesa, M., Linnemann, U., Hofmann, M., Gärtner, A., 2016. Detrital zircons from the Ordovician rocks of the Pyrenees: Geochronological constraints and provenance. Tectonophysics 681, 124–134. https://doi.org/10.1016/j.tecto.2016.03.015.
Martinez, A., Vergés, J., Clavell, E., Kennedy, J., 1989. Stratigraphic framework of the thrust geometry and structural inversion in the southeastern Pyrenees: La Garrotxa area. Geodin. Acta 3, 185–194. https://doi.org/10.1080/09853111.1989.11105185.
Marzoli, A., Renne, P.R., Piccirillo, E.M., Ernesto, M., Bellieni, G., Min, A.D., 1999. Extensive 200-Million-Year-Old Continental Flood Basalts of the Central Atlantic Magmatic Province. Science 284, 616–618. https://doi.org/10.1126/science.284.5414.616.
Mató, E., Saula, E., Martinez, A., Mmioz, J. A., Vergés, J. and Escuer, J. (1994) Memoria explicative y cartografa geologica de la Hoja 293 (Berga) del mapa geologic0 de Espafia Plan Magna a escala 1:50,000, I.T.G.E.
Maurel, O., Monie, P., Pik, R., Arnaud, N., Brunel, M., Jolivet, M., 2008. The Meso-Cenozoic thermo-tectonic evolution of the Eastern Pyrenees: an 40Ar/39Ar fission track and (U–Th)/He thermochronological study of the Canigou and Mont-Louis massifs. Int. J. Earth Sci. 97, 565–584.
Meinhold, G., 2010. Rutile and its applications in earth sciences. Earth Sci. Rev. 102, 1–28. https://doi.org/10.1016/j.earscirev.2010.06.001.
Metcalf, J.R., Fitzgerald, P.G., Baldwin, S.L., Muñoz, J.-A., 2009. Thermochronology of a convergent orogen: Constraints on the timing of thrust faulting and subsequent exhumation of the Maladeta Pluton in the Central Pyrenean Axial Zone. Earth Planet. Sci. Lett. 287, 488–503.
Mey, P.H.W., Nagtegaal, P.J.C., Roberti, K.J., Hartevelt, J.J.A., 1968. Lithostratigraphic subdivision of post-Hercynian deposits in the south-central Pyrenees, Spain. Leidse. Geol. Meded. 41, 221–228.
Mouthereau, F., Filleaudeau, P.-Y., Vacherat, A., Pik, R., Lacombe, O., Fellin, M.G., Castelltort, S., Christophoul, F., Masini, E., 2014. Placing limits to shortening evolution in the Pyrenees: Role of margin architecture and implications for the Iberia/Europe convergence. Tectonics 33, 2283–2314.
Muñoz, J.A., 1985. Estructura alpina i herciniana a la vora sud de la zona axial del Pirineu oriental. Servei Geològic de Catalunya.
Muñoz, J.A., 1992. Evolution of a continental collision belt: ECORS-Pyrenees crustal balanced cross-section. In: Thrust Tectonics. Springer, Pp. pp. 235–246.
Muñoz, J.A., Martinez, A., Vergés, J., 1986. Thrust sequences in the eastern Spanish Pyrenees. Journal of Structural Geology, International conference on trusting and deformation 8, 399–405. https://doi.org/10.1016/0191-8141(86)90058-1.
Odlum, M.L., Stockli, D.F., 2019. Thermotectonic evolution of the North Pyrenean Agly Massif during early cretaceous hyperextension using multi-mineral U-Pb thermochronometry. Tectonics. https://doi.org/10.1029/2018TC005298.
Olivier, P., Gleizes, G., Paquette, J.L., 2004. Gneiss domes and granite emplacement in an obliquely convergent regime: New interpretation of the Variscan Agly Massif (Eastern

Pyrenees, France). In: Special Papers-Geological Society of America, pp. 229–242.
Olivier, P., Gleizes, G., Paquette, J.L., Sáez, C.M., 2008. Structure and U–Pb dating of the Saint-Arnac pluton and the Ansignan charnockite (Agly Massif): a cross-section from the upper to the middle crust of the Variscan Eastern Pyrenees. J. Geol. Soc. 165 (1), 141–152.
Oms, O., Fondevilla, V., Riera, V., Marmi, J., Vicens, E., Estrada, R., Anadón, P., Vila, B., Galobart, À., 2016. Transitional environments of the lower Maastrichtian South-Pyrenean Basin (Catalonia, Spain): the Fumanya Member tidal flat. Cretac. Res. 57, 428–442. https://doi.org/10.1016/j.cretres.2015.09.004.
Perez, N.D., Horton, B.K., Carlotto, V., 2016. Structural inheritance and selective re-activation in the central Andes: Cenozoic deformation guided by pre-Andean structures in southern Peru. Tectonophysics 671, 264–280. https://doi.org/10.1016/j.tecto.2015.12.031.
Puigdefàbregas, C., Souquet, P., 1986. Tecto-sedimentary cycles and depositional sequences of the Mesozoic and Tertiary from the Pyrenees. Tectonophysics 129, 173–203.
Puigdefàbregas, C., Muñoz, J.A., Marzo, M., 1986. Thrust belt development in the Eastern Pyrenees and related depositional sequences in the southern Foreland Basin. In: Foreland Basins. John Wiley & Sons, Ltd, pp. 229–246. https://doi.org/10.1002/9781444303810.ch12.
Puigdefàbregas, C., Muñoz, J.A., Vergés, J., 1992. Thrusting and foreland basin evolution in the Southern Pyrenees. In: McClay, K.R. (Ed.), Thrust Tectonics. Springer Netherlands, Dordrecht, pp. 247–254. https://doi.org/10.1007/978-94-011-3066-0_22.
Ramos, E., Busquets, P., Vergés, J., 2002. Interplay between longitudinal fluvial and transverse alluvial fan systems and growing thrusts in a piggyback basin (SE Pyrenees). Sediment. Geol. 146, 105–131. https://doi.org/10.1016/S0037-0738(01)00169-5.
Reiners, P.W., 2005. Zircon (U-Th)/He thermochronometry. Rev. Mineral. Geochem. 58, 151–179. https://doi.org/10.2138/rmg.2005.58.6.
Reiners, P. W., Campbell, I. H., Nicolescu, S., Allen, C. M., Hourigan, J. K., Garver, J. I., & Cowan, D. S. (2005). (U-Th)/(He-Pb) double dating of detrital zircons. American Journal of Science, 305(4), 259[HYPHEN]311.
Respaut, J.P., Lancelot, J.R., 1983. Datation de la mise en place synmetamorphe de la charnockite d'Ansignan (massif de l'Agly) par la methode U/Pb sur zircons et monazites. In: Neues Jahrbuch fur Mineralogie, Abhandlungen. v. 147, n. 1. pp. 21–34.
Riba, O., 1976. Syntectonic unconformities of the Alto Cardener, Spanish Pyrenees: a genetic interpretation. Sediment. Geol. 15, 213–233. https://doi.org/10.1016/0037-0738(76)90017-8.
Riera, V., Marmi, J., Oms, O., Gomez, B., 2010. Orientated plant fragments revealing tidal palaeocurrents in the Fumanya mudflat (Maastrichtian, southern Pyrenees): Insights in palaeogeographic reconstructions. Palaeogeogr. Palaeoclimatol. Palaeoecol. 288, 82–92. https://doi.org/10.1016/j.palaeo.2010.01.037.
Roca, E., Sans, M., Cabrera, L., Marzo, M., 1999. Oligocene to Middle Miocene evolution of the central Catalan margin (northwestern Mediterranean). Tectonophysics 315, 209–229. https://doi.org/10.1016/S0040-1951(99)00289-9.
Roca, E., Muñoz, J.A., Ferrer, O., Ellouz, N., 2011. The role of the Bay of Biscay Mesozoic extensional structure in the configuration of the Pyrenean orogen: Constraints from the MARCONI deep seismic reflection survey. Tectonics 30. https://doi.org/10.1029/2010TC002735.
Roigé, M, Gómez-Gras, D, Remacha, E, Boya, S, Viaplana-Muzas, M, Teixell, A, 2017. Recycling an uplifted early foreland basin fill: An example from the Jaca basin (Southern Pyrenees, Spain). Sedimentary geology 360, 1–21.
Roigé, M., Gómez-Gras, D., Remacha, E., Daza, R., Boya, S., 2016. Tectonic control on sediment sources in the Jaca basin (Middle and Upper Eocene of the South-Central Pyrenees). Compt. Rendus Geosci. 348, 236–245.
Romans, B.W., Fildani, A., Graham, S.A., Hubbard, S.M., Covault, J.A., 2010. Importance of predecessor basin history on sedimentary fill of a retroarc foreland basin: Provenance analysis of the Cretaceous Magallanes basin, Chile (50–52 S). Basin Res. 22, 640–658.
Rosenbaum, G., Lister, G.S., Duboz, C., 2002. Relative motions of Africa, Iberia and Europe during Alpine orogeny. Tectonophysics 359, 117–129.
Rossi, P., Cocherie, A., Fanning, C.M., Ternet, Y., 2003. Datation U-Pb sur zircons des dolérites tholéiitiques pyrénéennes (ophites) à la limite Trias–Jurassique et relations avec les tufs volcaniques dits “infra-liasiques” nord-pyrénéens. Compt. Rendus Geosci. 335, 1071–1080. https://doi.org/10.1016/j.crte.2003.09.011.
Roure, F, Choukroune, P, Berastegui, X, Munoz, JA, Villien, A, Matheron, P, Bareyt, M, Seguret, M, Camara, P, Deramond, J, 1989. ECORS deep seismic data and balanced cross sections: Geometric constraints on the evolution of the Pyrenees. Tectonics 8 (1), 41–50.
Saura, E., Teixell, A., 2006. Inversion of small basins: effects on structural variations at the leading edge of the Axial Zone antiformal stack (Southern Pyrenees, Spain). Journal of Structural Geology, Tectonic Inversion and Structural Inheritance in Mountain Belts 28, 1909–1920. https://doi.org/10.1016/j.jsg.2006.06.005.
Saylor, J.E., Stockli, D.F., Horton, B.K., Nie, J., Mora, A., 2012. Discriminating rapid exhumation from syndepositional volcanism using detrital zircon double dating: Implications for the tectonic history of the Eastern Cordillera, Colombia. Geol. Soc. Am. Bull. 124, 762–779.
Schoene, B., 2014. U–Th–Pb Geochronology. In: Treatise on Geochemistry. Elsevier, pp. 341–378. https://doi.org/10.1016/B978-0-08-095975-7.00310-7.
Séranne, M., 1999. The Gulf of Lion continental margin (NW Mediterranean) revisited by IBS: an overview. Geol. Soc. Lond., Spec. Publ. 156, 15–36. https://doi.org/10.1144/GSL.SP.1999.156.01.03.
Serra-Kiel, J., Canudo, J.I., Dinares, J., Molina, E., Ortiz, N., Pascual, J.O., ... Tosquella, J., 1994. Cronoestratigrafía de los sedimentos marinos del Terciario inferior de la Cuenca de Graus-Trem (Zona Central Surpirenaica). Rev. Soc. Geol. Esp. 7 (3–4), 273–295.
Serra-Kiel, J., Hottinger, L., Caus, E., Drobne, K., Ferrández, C., Jauhri, A.K., Less, G., Pavlovec, R., Pignatti, J., Samsó, J.M., Schaub, H., Sirel, E., Strougo, A., Tambareau, Y., Tosquella, J., Zakrevskaya, E., 1998. Larger foraminiferal biostratigraphy of the Tethyan Paleocene and Eocene. Bulletin de la Société Géologique de France 169 (2), 281–299.
Serra-Kiel, J., Mató, E., Saula, E., Travé, A., Ferràndez-Cañadell, C., Busquets, P., Samsó, J.M., Tosquella, J., Barnolas, A., Àlvarez-Pérez, G., Franquès, J., Romero, J., 2003. An inventory of the marine and transitional Middle/Upper Eocene deposits of the Southeastern Pyrenean Foreland Basin. In: Geologica Acta. NE Spain, pp. 29.
Sinclair, HD, Gibson, M, Naylor, M, Morris, RG, 2005. Asymmetric growth of the Pyrenees revealed through measurement and modeling of orogenic fluxes. American Journal of Science 305 (5), 369–406.
Smye, A.J., Marsh, J.H., Vermeesch, P., Garber, J.M., Stockli, D.F., 2018. Applications and limitations of U-Pb thermochronology to middle and lower crustal thermal histories. Chem. Geol. 494, 1–18. https://doi.org/10.1016/j.chemgeo.2018.07.003.
Solé, J., Pi, T., Enrique, P., 2003. New geochronological data on the Late Cretaceous alkaline magmatism of the northeast Iberian Peninsula. Cretac. Res. 24, 135–140.
Souriau, A., Chevrot, S., Olivera, C., 2008. A new tomographic image of the Pyrenean lithosphere from teleseismic data. Tectonophysics 460, 206–214. https://doi.org/10.1016/j.tecto.2008.08.014.
Stampfli, G.M., Borel, G.D., 2002. A plate tectonic model for the Paleozoic and Mesozoic constrained by dynamic plate boundaries and restored synthetic oceanic isochrons. Earth Planet. Sci. Lett. 196 (1), 17–33.
Suppe, J., Sàbat, F., Anton Muñoz, J., Poblet, J., Roca, E., Vergés, J., 1997. Bed-by-bed fold growth by kink-band migration: Sant llorenç de Morunys, eastern Pyrenees. Journal of Structural Geology, Fault-Related Folding 19, 443–461. https://doi.org/10.1016/S0191-8141(96)00103-4.
Teixell, A., 1998. Crustal structure and orogenic material budget in the west Central Pyrenees. Tectonics 17, 395–406.
Teixell, A., Labaume, P., Lagabrielle, Y., 2016. The crustal evolution of the west-central Pyrenees revisited: inferences from a new kinematic scenario. Compt. Rendus Geosci. 348, 257–267.
Teixell, A., Labaume, P., Ayarza, P., Espurt, N., de Saint Blanquat, M., Lagabrielle, Y., 2018. Crustal structure and evolution of the Pyrenean-Cantabrian belt: a review and new interpretations from recent concepts and data. Tectonophysics 724, 146–170.
Ternois, S., Odlum, M.L., Ford, M., Pik, R., Stockli, D.F., Tibari, B., Vacherat, A., Bernard, V., 2019. Thermochronological evidence of early orogenesis, eastern Pyrenees, France. Tectonics. https://doi.org/10.1029/2018TC005254.
Thomson, K.D., Stockli, D.F., Clark, J.D., Puigdefàbregas, C., Fildani, A., 2017. Detrital zircon (U-Th)/(He-Pb) double-dating constraints on provenance and foreland basin evolution of the Ainsa Basin, south-central Pyrenees, Spain: Ainsa Basin Zircon Double Dating. Tectonics 36, 1352–1375. https://doi.org/10.1002/2017TC004504.
Thomson, KD, Stockli, DF, Odlum, ML, Tolentino, P, Puigdefàbregas, C, Clark, J, Fildani, A, 2019. Sediment provenance and routing evolution in the Late Cretaceous -Eocene Ager Basin, south -central Pyrenees, Spain. *Basin Research*.. https://doi.org/10.1111/bre.12376.
Tomkins, HS, Powell, R, Ellis, DJ, 2007. The pressure dependence of the zirconium-in-rutile thermometer. Journal of metamorphic Geology 25 (6), 703–713.
Triebold, S., von Eynatten, H., Zack, T., 2012. A recipe for the use of rutile in sedimentary provenance analysis. Sedimentary Geology. The 2011 Tohoku-oki tsunami 282, 268–275. https://doi.org/10.1016/j.sedgeo.2012.09.008.
Tugend, J., Manatschal, G., Kusznir, N.J., 2015. Spatial and temporal evolution of hyperextended rift systems: Implication for the nature, kinematics, and timing of the Iberian-European plate boundary. Geology 43, 15–18. https://doi.org/10.1130/G36072.1.
Vacherat, A., Mouthereau, F., Pik, R., Bernet, M., Gautheron, C., Masini, E., Le Pourhiet, L., Tibari, B., Lahfid, A., 2014. Thermal imprint of rift-related processes in orogens as recorded in the Pyrenees. Earth Planet. Sci. Lett. 408, 296–306.
Vacherat, A., Mouthereau, F., Pik, R., Bellahsen, N., Gautheron, C., Bernet, M., Daudet, M., Balansa, J., Tibari, B., Pinna Jamme, R., Radal, J., 2016. Rift-to-collision transition recorded by tectonothermal evolution of the northern Pyrenees. Tectonics 35, 2015TC004016. https://doi.org/10.1002/2015TC004016.
Vacherat, A., Mouthereau, F., Pik, R., Huyghe, D., Paquette, J.-L., Christophoul, F., Loget, N., Tibari, B., 2017. Rift-to-collision sediment routing in the Pyrenees: a synthesis from sedimentological, geochronological and kinematic constraints. Earth Sci. Rev. 172, 43–74. https://doi.org/10.1016/j.earscirev.2017.07.004.
Van Dongen, P.G., 1967. The rotation of Spain: palaeomagnetic evidence from the eastern Pyrenees. Palaeogeogr. Palaeoclimatol. Palaeoecol. 3, 417–432.
Veizer, J., Prokoph, A., 2015. Temperatures and oxygen isotopic composition of Phanerozoic oceans. Earth Sci. Rev. 146, 92–104. https://doi.org/10.1016/j.earscirev.2015.03.008.
Vergés, J., 1993. Estudi geològic del vessant sud del Pirineu oriental i central. Evolució cinemàtica en 3D. PhD thesis. University of Barcelona, Spain.
Vergés, J., Muñoz, J.A., Martínez, A., 1992. South Pyrenean fold and thrust belt: The role of foreland evaporitic levels in thrust geometry. In: McClay, K.R. (Ed.), Thrust Tectonics. Springer Netherlands, Dordrecht, pp. 255–264. https://doi.org/10.1007/978-94-011-3066-0_23.
Vergés, J., Millán, H., Roca, E., Muñoz, J.A., Marzo, M., Cirés, J., Den Bezemer, T., Zoetemeijer, R., Cloetingh, S., 1995. Eastern Pyrenees and related foreland basins: pre-, syn- and post-collisional crustal-scale cross-sections. Mar. Pet. Geol. 12, 903–915.
Vergés, J, Burbank, DW, 1996. Eocene-Oligocene thrusting and basin configuration in the eastern and central Pyrenees (Spain). In: *Tertiary basins of Spain: the stratigraphic record of crustal kinematics*, 6, p. pp. 120.
Vergés, J., Marzo, M., Santaeulària, T., Serra-Kiel, J., Burbank, D.W., Muñoz, J.A.,

Giménez-Montsant, J., 1998. Quantified vertical motions and tectonic evolution of the SE Pyrenean foreland basin. Geol. Soc. Lond., Spec. Publ. 134, 107–134. https://doi.org/10.1144/GSL.SP.1998.134.01.06.

Vergés, J., Fernàndez, M., Martìnez, A., 2002. The Pyrenean orogen: pre-, syn-, and post-collisional evolution. J. Virtual Explor. 8, 55–74.

Vissers, R.L.M., 1992. Variscan extension in the Pyrenees. Tectonics 11, 1369–1384. https://doi.org/10.1029/92TC00823.

Vissers, R.L.M., Meijer, P.T., 2012. Mesozoic rotation of Iberia: subduction in the Pyrenees? Earth Sci. Rev. 110, 93–110.

Vitrac-Michard, A., Allègre, C.J., 1975. 238 U-206 Pb, 235 U-207 Pb, systematics on Pyrenean basement. Contrib. Mineral. Petrol. 51, 205–212.

Wang, Y., Chevrot, S., Monteiller, V., Komatitsch, D., Mouthereau, F., Manatschal, G., Sylvander, M., Diaz, J., Ruiz, M., Grimaud, F., Benahmed, S., Pauchet, H., Martin, R., 2016. The deep roots of the western Pyrenees revealed by full waveform inversion of teleseismic P waves. Geology 44, 475–478. https://doi.org/10.1130/G37812.1.

Whitchurch, A.L., Carter, A., Sinclair, H.D., Duller, R.A., Whittaker, A.C., Allen, P.A., 2011. Sediment routing system evolution within a diachronously uplifting orogen: Insights from detrital zircon thermochronological analyses from the South-Central Pyrenees. Am. J. Sci. 311, 442–482. https://doi.org/10.2475/05.2011.03.

Wolfe, M.R., Stockli, D.F., 2010. Zircon (U–Th)/He thermochronometry in the KTB drill hole, Germany, and its implications for bulk He diffusion kinetics in zircon. Earth Planet. Sci. Lett. 295, 69–82.

Zack, TV, Von Eynatten, H, Kronz, A, 2004. Rutile geochemistry and its potential use in quantitative provenance studies. Sedimentary Geology 171 (1-4), 37–58.

Zachos, J.C., Dickens, G.R., Zeebe, R.E., 2008. An early Cenozoic perspective on greenhouse warming and carbon-cycle dynamics. Nature 451, 279–283.

Zack, T., Stockli, D.F., Luvizotto, G.L., Barth, M.G., Belousova, E., Wolfe, M.R., Hinton, R.W., 2011. In situ U–Pb rutile dating by LA-ICP-MS: 208 Pb correction and prospects for geological applications. Contrib. Mineral. Petrol. 162, 515–530.